bioRxiv preprint doi: https://doi.org/10.1101/2021.03.08.433668; this version posted March 8, 2021. The copyright holder for this preprint (which was not certified by peer review) is the author/funder, who has granted bioRxiv a license to display the preprint in perpetuity. It is made available under aCC-BY-NC-ND 4.0 International license.

Integrative multi-omics profiling reveals cAMP-independent mechanisms regulating hyphal morphogenesis in *Candida albicans*

Kyunghun Min[1], Thomas F. Jannace[1,5], Haoyu Si[1,6], Krishna R. Veeramah[2], John D. Haley[3,4], and James B. Konopka[1]*

[1] Department of Microbiology and Immunology, Renaissance School of Medicine, Stony Brook University (SUNY), Stony Brook, NY, USA

[2] Department of Ecology and Evolution, Stony Brook University (SUNY), Stony Brook, NY, USA

[3] Department of Pathology, Renaissance School of Medicine, Stony Brook University (SUNY), Stony Brook, NY, USA

[4] Biological Mass Spectrometry Shared Resource, Renaissance School of Medicine, Stony Brook University (SUNY), Stony Brook, NY, USA

[5] Present address: Department of Quality Assurance, Biogen, Morrisville, NC, USA

[6] Present address: School of Biological Sciences, University of Nebraska-Lincoln, Lincoln, NE, USA

* Corresponding author: james.konopka@stonybrook.edu

bioRxiv preprint doi: https://doi.org/10.1101/2021.03.08.433668; this version posted March 8, 2021. The copyright holder for this preprint (which was not certified by peer review) is the author/funder, who has granted bioRxiv a license to display the preprint in perpetuity. It is made available under aCC-BY-NC-ND 4.0 International license.

ABSTRACT

Microbial pathogens grow in a wide range of different morphologies that provide distinct advantages for virulence. In the fungal pathogen *Candida albicans*, adenylyl cyclase (Cyr1) has been thought to be a master regulator of the switch to invasive hyphal morphogenesis and biofilm formation. However, faster growing *cyr1Δ*/Δ pseudorevertant (PR) mutants were identified that form hyphae in the absence of cAMP. Isolation of additional PR mutants revealed that their improved growth was due to loss of one copy of *BCY1*, the negative regulatory subunit of protein kinase A, from the left arm of chromosome 2. Furthermore, hyphal morphogenesis was improved in some of PR mutants by multigenic haploinsufficiency resulting from loss of large regions of the left arm of chromosome 2, including global transcriptional regulators. Interestingly, hyphal-associated genes were also induced in a manner that was independent of cAMP. This indicates that basal protein kinase A activity is an important prerequisite to induce hyphae, but activation of the cAMP pathway is not needed. Instead, phosphoproteomic analysis indicated that the Cdc28 cyclin-dependent kinase and the casein kinase Yck2 play key roles in promoting polarized growth. In addition, integrating transcriptomic and proteomic data reveals hyphal stimuli induce increased production of key transcription factors that contribute to polarized morphogenesis.

bioRxiv preprint doi: https://doi.org/10.1101/2021.03.08.433668; this version posted March 8, 2021. The copyright holder for this preprint (which was not certified by peer review) is the author/funder, who has granted bioRxiv a license to display the preprint in perpetuity. It is made available under aCC-BY-NC-ND 4.0 International license.

INTRODUCTION

Fungal pathogens are capable of transitioning between different morphologies that provide distinct advantages for virulence and survival in the host[1,2]. For example, the fungal pathogen *Candida albicans* switches from budding to hyphal growth, which promotes virulence as the long hyphal filaments mediate invasion into tissues, escape from immune cells, and biofilm formation[1-6]. A variety of stimuli promote hyphal morphogenesis, including serum, CO_2, alkaline pH, peptidoglycan breakdown products, N-acetylglucosamine (GlcNAc), and contact with a solid matrix[3,7,8]. In *C. albicans*, it has long been thought that adenylyl cyclase (Cyr1) is a master regulator of hyphal growth[3,5,9-11]. Deletion of adenylyl cyclase (*cyr1*Δ/Δ) blocks hyphal formation, and addition of millimolar levels of exogenous cAMP induces it[12]. However, interpreting the role of Cyr1 and cAMP is complicated by the fact that the *cyr1*Δ/Δ mutants grow very poorly[13]. Furthermore, a recent study showed that faster growing *cyr1*Δ/Δ pseudorevertant (PR) mutants form hyphae in the absence of Cyr1 and cAMP[14]. Thus, although cAMP is capable of inducing hyphae, it is not essential for most hyphal stimuli[14].

In *C. albicans*, cAMP formed from ATP by Cyr1 acts by binding to the negative regulatory subunit (Bcy1) of protein kinase A (PKA), thereby releasing the PKA catalytic subunits (Tpk1 and Tpk2) to phosphorylate target proteins[11]. Most current models propose that the cAMP-PKA pathway induces the expression of a special set of genes that promote hyphal growth[2,3,11,13,15,16]. This has been supported by the ability of many transcription factors (TFs) to regulate this switch. For example, PKA was reported to phosphorylate the Efg1 TF, which is required for hyphal induction[17,18]. However, transcriptional analysis of hyphal induced genes has not revealed the mechanism of hyphal induction[19,20]. The common core set of genes stimulated by a group of different hyphal inducers in *C. albicans* do not account for the transition to hyphal growth[19]. In addition, our recent studies showed that a mutant that cannot catabolize GlcNAc can be stimulated by GlcNAc to form hyphae without induction of hyphal-specific genes[20]. Other studies have shown that some hyphal regulatory TFs can be bypassed under

bioRxiv preprint doi: https://doi.org/10.1101/2021.03.08.433668; this version posted March 8, 2021. The copyright holder for this preprint (which was not certified by peer review) is the author/funder, who has granted bioRxiv a license to display the preprint in perpetuity. It is made available under aCC-BY-NC-ND 4.0 International license.

special conditions[21], such as altered expression of the Cak1 protein kinase[22] or in the absence of a variant histone H3[23]. This indicates that although TFs are important for creating the proper physiological environment for cells to undergo hyphal growth, the target genes are not directly involved in promoting filamentous morphogenesis.

Other studies have implicated several protein kinases that are not regulated by cAMP in hyphal signaling[2,3,24]. For example, the cyclin-dependent kinase Cdc28 promotes hyphal growth in part by phosphorylating several proteins involved in polarized morphogenesis[24-32]. Therefore, to better define the cAMP-dependent and independent mechanisms of hyphal signaling, we isolated a set of new *cyr1*Δ/Δ PR mutants that displayed variable levels of improved growth rates and ability to form hyphae. The wild type and PR mutant cells were compared with four omics approaches: genomics combined with gene-mapping by CRISPR-Cas9 to identify genetic changes in PR mutants, transcriptomics to better define the role of cAMP in hyphal gene regulation, proteomics and phosphoproteomics to reveal key kinases for hyphal induction. Furthermore, integrative transcriptomics and proteomics profiling indicates that there are increases in the levels of key transcription factors, possibly due to changes in their translation rate, that are induced by hyphal signaling. Altogether, these results reveal how multiple processes in the gene expression pathway can modulate cellular differentiation.

RESULTS

Large deletions in the left arm of chromosome 2 bypass the need for cAMP to improve the growth rate and to stimulate hyphal morphogenesis.

We previously reported that slow growing *cyr1*Δ/Δ mutant strains give rise to faster growing cells, which we termed pseudorevertants (PRs)[14]. Interestingly, these spontaneous PRs could form hyphae even though they lack Cyr1 and cAMP[14]. To better define the underlying mechanisms, we isolated additional PR strains and found that they differed in their growth rates and ability to be induced to form hyphae (Fig. 1a,b and Supplementary Fig. 1).

bioRxiv preprint doi: https://doi.org/10.1101/2021.03.08.433668; this version posted March 8, 2021. The copyright holder for this preprint (which was not certified by peer review) is the author/funder, who has granted bioRxiv a license to display the preprint in perpetuity. It is made available under aCC-BY-NC-ND 4.0 International license.

Based on these phenotypic differences, the new PR mutants could be grouped into 4 classes (Table 1). Surprisingly, the degree of improved growth rate of the PR mutants did not correlate with their ability to form hyphae, indicating that the mechanisms of suppression were complex. The faster growing Class 1 mutant doubled at a nearly wild-type rate (1.5 h) but only 74% of the cells formed hyphae. In contrast, the Class 2, Class 3, and Class 3+ PR mutants grew slower than the Class 1 mutants but were more efficient at forming hyphae. For example, Class 3 mutants grew at a doubling time of 2.3 h yet 93% of the cells could form hyphae.

Whole genome sequencing of the diploid *C. albicans* strains identified distinct genetic changes in the four classes of PR mutants. Interestingly, although they were different, all four classes of mutants contained genetic changes that resulted in loss of expression of one copy of *BCY1*, which encodes the negative regulatory subunit of cAMP-dependent PKA kinase. This suggested that reduced expression of *BCY1* increased PKA activity resulting in improved growth in the absence of cAMP. Similar results reported that a *bcy1*Δ mutant can rescue growth of a *cyr1*Δ mutant in *S. cerevisiae*[33]. Class 1 mutants exhibited the simplest genetic change, in that the improved growth correlated with a premature stop codon in *BCY1* on chromosome 2 (Fig. 1c, Extended data Table 1, and Source data 1). In contrast, the Class 2, 3, and 3+ PR mutants all lacked part of the left arm of one copy of chromosome 2 that includes *BCY1*.

Western blot analysis showed that the Bcy1 protein levels were reduced by 50% in the PR mutants, confirming that altered gene dosage leads to reduced production of Bcy1 (Extended Data Fig. 1). The reduction in Bcy1 did not impact the levels of Tpk2, one of the PKA catalytic subunits in the PR mutants compared to the WT. Interestingly, *TPK2* was located in the middle of the chromosome 2, which was duplicated in Class 3+ PRs. However, none of the other PKA pathway components were located on chromosome 2. This supports the conclusion that the haploinsufficiency of *BCY1* bypassed the need for cAMP for growth and hyphal induction in *C. albicans*.

bioRxiv preprint doi: https://doi.org/10.1101/2021.03.08.433668; this version posted March 8, 2021. The copyright holder for this preprint (which was not certified by peer review) is the author/funder, who has granted bioRxiv a license to display the preprint in perpetuity. It is made available under aCC-BY-NC-ND 4.0 International license.

In the Class 2 and 3+ PRs, similar breakpoints were identified in the independently isolated strains indicating that a specific DNA sequence induced the chromosomal deletion. To better understand how the large deletions of 270 kb and 590 kb were generated in the Class 2, 3, and 3+ PRs, we inspected the genome sequences for matches to the *C. albicans* 23-bp telomere repeat sequence (CACCAAGAAGTTAGACATCCGTA)[34] , which was found at the deletion end points (Extended Data Table 1). Analysis of the breakpoint regions in chromosome 2 revealed 4 to 9-bp matches to telomere seed sequences. However, the long repeat sequence, which was previously reported to drive genome rearrangements, was not found near the deletion sites[35]. As described previously, this suggests that chromosome break healing by *de novo* telomere addition contributes to the genome plasticity in *C. albicans*[36,37,38], which enables it to adapt to adverse conditions or deleterious mutations such as *cyr1*Δ/Δ.

Gene mapping by CRISPR-Cas9 identified general transcription factors are involved in hyphal regulation.

To confirm that the genetic changes in chromosome 2 improved growth and hyphal induction in the PR mutants, transient expression of the CRISPR-Cas9 system[39,40] was utilized to recreate the loss of one copy of *BCY1* and the large deletions present in the Class 2, 3, and 3+ PR mutants. To facilitate large deletions, two single guide RNAs (sgRNAs) were used to target Cas9 to cut immediately adjacent to the deletion end points detected in the spontaneous PR mutants (Fig. 2a). Analysis of these *cyr1*Δ/Δ mutants that were created to be heterozygous *bcy1*Δ, 270kbΔ, and 590kbΔ in chromosome 2 showed that they recapitulated the phenotypes of the corresponding spontaneous mutants PR13, PR12, and PR18, respectively (Fig. 2b,c,d). This confirmed that haploinsufficiency of *BCY1* improved growth, and that haploinsufficiency of the genes in the 270 kb region in the left arm of chromosome 2 was sufficient to improve hyphal induction in the PR mutants.

bioRxiv preprint doi: https://doi.org/10.1101/2021.03.08.433668; this version posted March 8, 2021. The copyright holder for this preprint (which was not certified by peer review) is the author/funder, who has granted bioRxiv a license to display the preprint in perpetuity. It is made available under aCC-BY-NC-ND 4.0 International license.

Gene mapping strategies to identify the basis for the improved hyphal growth of the PR mutants showed that this effect is due to multiple genetic changes (Fig. 2e). In the first approach, smaller 90 kb sections of the 270 kb region were deleted from one copy of chromosome 2 in a *bcy1*Δ *cyr1*Δ/Δ strain. However, these mutants were not better at producing filamentous hyphal cells than the parental strain, suggesting that the improved hyphal morphogenesis is multigenic. Heterozygous deletion of a larger segment of chromosome 2 from 90kb→260kb made the cells more filamentous, which partially narrowed the key region. Smaller deletions designed to map the right end of the critical region of chromosome 2 showed that a 90kb→250kb deletion mutant did not exhibit better hyphal growth. Haploinsufficiency of the 10-kb region was therefore necessary to improve hyphal induction (although it was not sufficient on its own). Further mapping by deletion of the genes in this 10-kb region identified *SRB9* and *SPT5* to be involved in the improved hyphal phenotype (Extended Data Fig. 2). *SRB9* encodes a subunit of the RNA polymerase II mediator complex and *SPT5* encodes a transcription elongation factor complex subunit. Interestingly, the double heterozygous mutation of *SRB9* and *SPT5* in the 90kb→250kb deletion strain promoted improved hyphal growth, while the single heterozygous mutations of each gene did not. Thus, the gene mapping results indicate that global transcriptional regulators are important for creating a physiological state in the cell that is more conducive to induction of the switch of hyphal morphogenesis. This finding is consistent with the previous study[41] that protein components of Mediator, an important transcriptional coregulatory protein complex, were highly phosphorylated in *C. albicans* hyphae.

cAMP signaling is not necessary for transcriptional induction of hyphal regulated genes

Based in part on previous studies of *cyr1*Δ/Δ mutant strains, cAMP signaling was thought to be central to inducing the expression of a variety of genes, including virulence factors such as adhesins and hyphal-specific genes that promote filamentous growth[2,3,13,15,16]. To examine this role of cAMP signaling, we performed RNA sequencing (RNA-seq) analysis of the

bioRxiv preprint doi: https://doi.org/10.1101/2021.03.08.433668; this version posted March 8, 2021. The copyright holder for this preprint (which was not certified by peer review) is the author/funder, who has granted bioRxiv a license to display the preprint in perpetuity. It is made available under aCC-BY-NC-ND 4.0 International license.

WT and PR mutants before and after stimulation with the hyphal inducer GlcNAc (Fig. 3a and Source Data 2). Heatmap clustering and principal component analysis (PCA) of the normalized RNA-seq dataset revealed that WT and PRs showed similar patterns in transcriptomes, indicating that cAMP is not required to induce the broad range of hyphal genes (Fig. 3b and Supplementary Fig. 2). In contrast, the *cyr1*Δ/Δ mutant clustered separately due to its expected defect in regulating hyphal genes (Fig. 3b). Data for a subset of hyphal genes, as well as controls are shown in Fig. 3c. The transcriptomic profile of PR13 (*bcy1**/*BCY1 cyr1*Δ/Δ) was highly similar to the WT. However, PR12 (270kbΔ *cyr1*Δ/Δ) expressed a higher basal level of hyphal genes even in the absence of the hyphal inducer GlcNAc (Fig. 3c), which also correlates with a higher basal level of filamentous cell morphology (Fig. 1b). The PR12 transcriptome was also distinct as the levels of the genes in the 270-kb region were around 2-fold less than the WT level due to the haploinsufficiency (see Source Data 2). GlcNAc catabolic genes were highly expressed in all the strains tested, including *cyr1*Δ/Δ (Fig. 3c), which is consistent with previous studies showing that their regulation is cAMP independent[42,43]. Altogether, these data indicate that an appropriate basal level of PKA activity is needed for cells to respond transcriptionally to a hyphal inducer, rather than a requirement for stimulation of Cyr1 to produce cAMP.

Quantitative phosphoproteomics identified protein kinases required for normal hyphal growth

To better understand how the switch to hyphal morphogenesis is regulated, we compared protein production and phosphorylation during hyphal induction. WT and PR13 strains were treated with or without GlcNAc to form hyphae (Fig. 4a), and then a label-free mass spectrometry approach (LC-MS/MS) was used to detect 3,434 proteins and 17,580 phosphopeptides (Source Data 3). To differentiate experimental variances from biological alterations, we compared the replicate data of WT cells treated with GlcNAc from both the whole proteome and the phosphoproteome. The null comparisons of the biological replicates showed

bioRxiv preprint doi: https://doi.org/10.1101/2021.03.08.433668; this version posted March 8, 2021. The copyright holder for this preprint (which was not certified by peer review) is the author/funder, who has granted bioRxiv a license to display the preprint in perpetuity. It is made available under aCC-BY-NC-ND 4.0 International license.

high correlations (r > 0.9) (Fig. 4b). Efg1 was reported as a target of PKA and CDC28 kinases and the genetic studies implicated that T179 and T206 positions were the phosphosites[17,32]. However, phosphoproteome data did not detect the previously reported phosphosites in consistent with the reports of Willger et al.[41] and Cao et al.[44] (see Source Data 3). This suggests that the phosphorylation mechanism of Efg1 is different from the previous models. Interestingly, Efg1 was dephosphorylated during hyphal induction in the C-terminal prion-like domain (PrLD), which supports the assembly of TF complexes by formation of phase-separated condensates[45].

We next used gene set enrichment analysis[46] to infer the activity of specific protein kinases. The algorithm was based on the levels of phosphorylated peptides containing amino acid sequence motifs characteristic of the substrate specificity of known protein kinases (Fig. 4c). Strikingly, in contrast to the current models[2,3,5], this analysis revealed PKA activity was not significantly different before and after hyphal induction in the WT or PR13 strains (Fig. 4d). Furthermore, control studies showed that PKA subunit (Bcy1 and Tpk2) levels remained constant during hyphal induction (Extended Data Fig. 1). Thus, there was no evidence to support the stimulation of PKA in the PR mutants during hyphal induction. In contrast, Cdc28 kinase activity was increased during hyphal induction in the WT strain (Fig. 4d), consistent with previous studies implicating this cyclin dependent kinase in hyphal regulation[25,26,32,47]. To examine the role of Cdc28 further, we deleted the hyphal-induced cyclin *HGC1*. The *hgc1*Δ/Δ mutation caused a stronger hyphal defect in the PR13 mutant compared to the WT control cells (Extended Data Fig. 3a), indicating that PR13 cells are more reliant on cyclin-dependent activity for hyphal induction than are the WT cells.

Interestingly, many of the Cdc28 phosphosites also contained a second motif indicating they are targets for yeast casein kinase 1 (Yck2) (Fig. 4e,f,g). Recent studies in *C. albicans* have characterized the role of Yck2 in modulating morphogenesis, virulence, fungal cell-wall stress responses, and resistance to clinical antifungals[48-50]. Deletion of *YCK2* strongly affected

bioRxiv preprint doi: https://doi.org/10.1101/2021.03.08.433668; this version posted March 8, 2021. The copyright holder for this preprint (which was not certified by peer review) is the author/funder, who has granted bioRxiv a license to display the preprint in perpetuity. It is made available under aCC-BY-NC-ND 4.0 International license.

hyphal growth in both the WT and PR13 strains (Extended Data Fig. 3a). The *yck2*Δ/Δ cells displayed an elongated cell morphology, but did not switch to a true hyphal morphology in the presence of the hyphal inducers serum or GlcNAc. Interestingly, both kinases phosphorylated 11 sites in 8 genes and they are all thought to have a role in polarized growth (Extended Data Table 2). We created phospho-site mutations of *BNI1* and *MOB2* because they were required for normal hyphal growth[30,51]. However, phospho-mutation of the individual phosphorylation sites did not cause any hyphal defect, suggesting that it may require mutations of additional target proteins to cause a strong defect in hyphal morphogenesis (Extended Data Fig. 3b).

Hyphal stimulation induces translation of TFs that regulate morphological switching

The transcriptomic and proteomic data sets were examined to determine how the abundance of mRNAs and their corresponding proteins correlated during the switch to hyphal morphogenesis. There was a relatively weak correlation (Pearson correlation coefficient, r = 0.39) between mRNA and protein abundances in *C. albicans* (Fig. 5b). Typical Pearson correlation coefficients (r) for mammalian cells are about 0.6 and *S. cerevisiae* is about 0.7[52]. This indicated that *C. albicans* has dynamic post-transcriptional regulatory mechanisms. Since protein levels are a function of mRNA abundance, translation rate, and protein turnover (Fig. 5a), we approximated the translation rate with the protein/mRNA level ratio (this approximation neglects protein degradation, see Fig. 5c). Integration of RNA-seq and label-free LC-MS/MS data gave an opportunity to estimate the translation rate of 3267 genes (Source Data 4). The translation rate spanned over five orders of magnitude across genes (Fig. 5d). There was a negative correlation between mRNA abundance and translation rate, while there was a positive correlation between protein abundance and translation rate. Although it has been reported that 5' UTR length plays an important role in translation efficiency[53-55], there was no correlation between 5' UTR length and translation rate in our analysis.

bioRxiv preprint doi: https://doi.org/10.1101/2021.03.08.433668; this version posted March 8, 2021. The copyright holder for this preprint (which was not certified by peer review) is the author/funder, who has granted bioRxiv a license to display the preprint in perpetuity. It is made available under aCC-BY-NC-ND 4.0 International license.

We next examined whether the translation rate changed for TFs that are known to regulate hyphal morphogenesis. Strikingly, translation rates of some hyphal regulator TFs increased dramatically during hyphal growth while the mean translation rates of ribosomal proteins and total proteins were similar (Fig. 5e). However, mRNA levels of the hyphal regulator TFs did not change much compared to the translation rate (Fig. 5f). The Ume6, Sfl1, Brg1, Tec1, and Fkh2 proteins were not detected in the uninduced cells while their mRNA levels were similar to the median of total mRNAs (Source Data 4). Further work will be required to confirm whether these effects are due to translation or another mechanism, such as increased protein stability[56,57]. However, the results demonstrate that a post-transcriptional mechanism regulates key transcription factors that are important for hyphal morphogenesis.

DISCUSSION

The ability of *C. albicans* to switch between budding and hyphal morphologies contributes to virulence by promoting invasive growth, escape from immune cells, and biofilm formation[1-6]. The prevailing model has been that adenylyl cyclase acts as a master regulator by integrating signals from different hyphal inducers[3,5,9-11]. Although high levels of exogenous cAMP[12] or hyperactive *CYR1* mutants[58] can induce filamentous growth, the failure of *cyr1*Δ/Δ cells to form hyphae does not provide strong support for an essential role of adenylyl cyclase as this mutant displays abnormal physiological properties and grows slowly[12-14]. Furthermore, treatment of *cyr1*Δ/Δ cells with low levels of cAMP to improve their growth enabled them to be stimulated to form hyphae[12,14]. Isolation of *cyr1*Δ/Δ PR mutants provided strong proof that inducers including serum, GlcNAc, and alkaline pH can stimulate hyphae in the total absence of cAMP[14]. We therefore identified the underlying mechanisms for this by demonstrating that the improved growth of the PR mutants is due to mutation or deletion of one of the two copies of *BCY1*, which encodes the negative regulatory subunit of PKA (Fig.1 and Fig. 2). The lower level of Bcy1 in the PR mutants was confirmed by Western blot analysis (Extended Data Fig. 1)

bioRxiv preprint doi: https://doi.org/10.1101/2021.03.08.433668; this version posted March 8, 2021. The copyright holder for this preprint (which was not certified by peer review) is the author/funder, who has granted bioRxiv a license to display the preprint in perpetuity. It is made available under aCC-BY-NC-ND 4.0 International license.

and RNA-seq data (Fig. 3). Consistent with this, the PR mutants grew better and displayed a transcriptomic profile similar to WT cells. These results are also interesting in that genomic analysis revealed that the different classes of PR mutants showed distinct mechanisms for mutation of *BCY1* or deletion of parts of the left arm of chromosome 2 (Extended Data Table 1), which underscore how the plasticity of the *C. albicans* genome enables it to adapt to different kinds of stress from mutations or antifungal drugs[35,36,59,60].

Current models also predict that PKA phosphorylates the Efg1 TF to stimulate it to induce expression of hyphal genes[2,3,11,13,15,16]. However, we failed to detect phosphorylation of Efg1 in WT or PR13 cells, consistent with previous studies[41,44]. In spite of this, the PR mutants were not only able to form hyphae, but they also induced the expression of the expected set of hyphal associated genes that includes many virulence factors (Fig. 3c). A further limitation of the current models is that several studies now question the role of transcriptional induction in promoting hyphal growth. For example, the common core set of genes stimulated by a group of different hyphal inducers in *C. albicans* do not account for the transition to hyphal growth[19]. In addition, under certain conditions GlcNAc can stimulate hyphae without induction of hyphal-specific genes[20]. There also appears to be a lack of TF specificity, as some hyphal regulatory TFs can be bypassed under special conditions[21], such as altered expression of the Cak1 protein kinase[22] or the absence of a variant histone H3[23]. In addition, filamentous growth is induced by deletion of the global transcriptional repressor *TUP1*[61]. Consistent with this, we found that haploinsufficiency of two global transcriptional regulators, *SRB9* and *SPT5*, contributed to the improved filamentous growth of the Class 2 mutants (Extended Data Fig. 2). Altogether, these data suggest a new model that TFs are important for creating the proper physiological environment for cells to undergo hyphal growth, but that the target genes are not directly involved in promoting filamentous morphogenesis.

To identify new mechanisms that promote hyphal growth, we carried out a multi-omics comparison of WT and PR cells (Extended Data Fig. 4). The phosphoproteomics analysis

bioRxiv preprint doi: https://doi.org/10.1101/2021.03.08.433668; this version posted March 8, 2021. The copyright holder for this preprint (which was not certified by peer review) is the author/funder, who has granted bioRxiv a license to display the preprint in perpetuity. It is made available under aCC-BY-NC-ND 4.0 International license.

identified a role of the Cdc28 cyclin dependent kinase and the Yck2 casein kinase 1 (Fig. 4). In fact, a subset of 8 proteins was dually phosphorylated by these protein kinases, although mutation of the phosphosites in two of these proteins (Bni1 and Mob2) did not cause a significant phenotype, perhaps because there are redundant mechanisms that contribute to hyphal growth (Extended Data Table 2 and Extended Data Fig. 3). Interestingly, deletion of *HGC1*, the hyphal-induced cyclin subunit of Cdc28, caused stronger defects in PR13 than in WT cells, suggesting that Cdc28 activity is more important for cAMP-independent induction of hyphal morphogenesis. In addition, integrative analysis of transcriptomic and proteomic data revealed that a set of transcription factors that are important for hyphal induction are produced at higher levels relative to their mRNA levels after hyphal induction, suggesting that differential translation of these factors represents a novel mechanism that contributes to hyphal growth (Fig. 5). Altogether, theses results indicate that future studies on hyphal signaling should focus on the roles that post-transcriptional and post-translational regulation play in promoting the changes in the morphogenesis pathways that mediate highly polarized hyphal growth.

METHODS

Strains, culture conditions, and hyphal analysis

The *C. albicans* strains used in this study are described in Supplementary Table 1. *C. albicans* strains were streaked fresh from storage at -80°C onto YPD (1% yeast extract, 2% peptone, 2% glucose) agar plates and then grown in rich YPD medium or in complete synthetic medium (SC) made with yeast nitrogen base, select amino acids, and uridine. *C. albicans* transformants were selected on YPD plus 200 µg/ml nourseothricin (NAT; Gold Biotechnology). NAT-sensitive derivatives of cells carrying the SAT flipper were then obtained by growing cells on maltose agar medium (1% yeast extract, 2% peptone, 2% maltose) for 2 days, and then several colonies were spread on YPD plates containing 25 µg/ml of NAT and incubated for 2

bioRxiv preprint doi: https://doi.org/10.1101/2021.03.08.433668; this version posted March 8, 2021. The copyright holder for this preprint (which was not certified by peer review) is the author/funder, who has granted bioRxiv a license to display the preprint in perpetuity. It is made available under aCC-BY-NC-ND 4.0 International license.

322 days at 30°C[40]. NAT-sensitive cells formed smaller colonies than NAT-resistant parental
323 strains.

324 Strain doubling times were determined from growth curves in YPD at 30°C. Fresh
325 overnight cultures were diluted to a final concentration of ~0.05 OD_{660} in 5 ml YPD in test tubes
326 and then incubated at 30°C on a tube roller. The OD_{660} was measured hourly for ~8 hours until
327 OD_{660} was >1.0. The reported doubling times are the averages of two biological replicates each
328 performed in duplicate.

329 To analyze hyphal formation in liquid media, cells were grown overnight at 30°C in YPD,
330 and then inoculated into SC + 50 mM glucose + 10% bovine calf serum, or SC + 50 mM GlcNAc
331 medium. Samples were then incubated at 37°C for the indicated time and then images were
332 captured using a Zeiss Axio Observer 7 inverted microscope equipped with a 40× objective
333 differential interference contrast (DIC) optics and a Zeiss AxioCam 702 digital camera. *C.*
334 *albicans* cells were grown and induced to make hyphae in the same conditions for
335 transcriptome, proteome, and phosphoproteome analyses. *C. albicans* cells were grown at
336 37°C to log phase (OD_{660} of 0.2 ~ 0.4) in SC + 50 mM galactose medium. For hyphal induction,
337 pre-warmed 0.5 M GlcNAc solution was added into the culture to make final concentration of 50
338 mM and the cultures were incubated for 2 h at 37°C. Cells were harvested by centrifugation,
339 washed three times with ice-cold ultrapure water, snap frozen on dry ice, and stored at −80°C.
340 Replicate experiments were conducted independently on different days.

341

342 **Strain construction**

343 Deletion mutant strains were created using transient expression of CRISPR-Cas9 to
344 facilitate the genome engineering and limit transformation-induced genomic changes in *C.*
345 *albicans*[39,62]. The methods were performed essentially as described previously[39,63]. Briefly,
346 *CaCAS9* expression and sgRNA expression cassettes were co-transformed into cells along with
347 a repair template. The *CaCAS9* gene was codon optimized for expression in *C. albicans*[64]. The

bioRxiv preprint doi: https://doi.org/10.1101/2021.03.08.433668; this version posted March 8, 2021. The copyright holder for this preprint (which was not certified by peer review) is the author/funder, who has granted bioRxiv a license to display the preprint in perpetuity. It is made available under aCC-BY-NC-ND 4.0 International license.

CaCAS9 expression cassette was PCR amplified from the plasmid pV1093, which was a kind gift from Dr. Valmik Vyas[64]. The sgRNA expression cassette was constructed through single-joint PCR from the plasmid pV1093[39]. We used 20-bp target sequences of the sgRNA, as reported previously by Vyas et al.[65] to target Cas9 to make a DNA double strand break at the target site (Supplementary Methods). When deleting large regions of chromosome 2 for gene mapping, two sgRNAs were used to cut each side of the target region. Repair templates were synthesized using the plasmid pGR-NAT as a template, which contains the *SAT1* flipper cassette[40]. The primers were designed to include 60 to 80 bases of homology to the sequences upstream or downstream from the target region. The oligonucleotides used in this study are listed in Supplementary Methods. PCR was conducted with Ex Taq (TaKaRa Bio, Inc.) in accordance with the CRISPR protocol (Supplementary Methods).

BNI1 and *MOB2* were mutated to prevent phosphorylation at the indicated sites using the CRISPR-Cas9 method developed by Vyas et al.[64] The 20-bp target sequence of sgRNA was cloned into pV1093 and correct clones were verified by DNA sequencing. The CRISPR expression plasmids were linearized by digestion with *Kpn1* and *Sac1* before transformation for efficient targeting to the *ENO1* locus. Repair templates were generated with two 60-base oligonucleotides containing a 20-base overlap at their 3′ ends centered on the desired site to mutate a phosphorylation site. The repair templates were constructed by PCR primer extension to contain the desired phospho-site mutation as well as a unique restriction site facilitate identification of appropriate transformants.

PCR products and linearized plasmids for transformation were purified and concentrated using a GeneJET PCR purification kit (Thermo Fisher Scientific, Inc.). Electroporation was used to introduce the DNA into cells following a previously described method[66]. An electrocompetent cell suspension (40 μl) was added to aliquoted DNA, placed in 0.1 cm-gap electroporation cuvettes, and electroporated on a Bio-Rad Gene Pulser at 1.5 kV. One milliliter of 0.5× YPD

bioRxiv preprint doi: https://doi.org/10.1101/2021.03.08.433668; this version posted March 8, 2021. The copyright holder for this preprint (which was not certified by peer review) is the author/funder, who has granted bioRxiv a license to display the preprint in perpetuity. It is made available under aCC-BY-NC-ND 4.0 International license.

373 containing 1 M sorbitol was added immediately to the cuvette, and then the cell mixture was
374 incubated for 3 h at 30°C before plating onto YPD + 200 µg/ml NAT agar. Nat^r transformants
375 were selected, and PCR genotyping of the transformants verified the genome editing.
376
377 **Genome analysis**
378 A 1 µg aliquot of the genomic DNA was prepared using the Illumina TruSeq PCR-free
379 DNA HT sample preparation kit with 450 bp insert size. Intact genomic DNA was sheared using
380 the Covaris sonicator (adaptive focused acoustics), followed by end-repair and bead-based size
381 selection of fragmented molecules. The size selected fragments then had adenines added to
382 the 3' ends of the DNA, Illumina sequence adaptors ligated onto the fragments, followed by
383 PCR amplification and final library QC. A majority of the steps in this process were performed
384 on the Caliper SciClone NGSx workstation (PerkinElmer), a robotics system developed and
385 validated for automated library preparation. The library QC included a measurement of the
386 average size of library fragments using the Agilent BioAnalyzer, estimation of the total
387 concentration of DNA by PicoGreen (ThermoFisher), and a measurement of the yield and
388 efficiency of the adaptor ligation process with a quantitative PCR assay (Kapa) using primers
389 specific to the adaptor sequence. Sequencing was performed on the Illumina MiSeq instrument
390 at 2 × 150 bp read length.
391 Reads were first trimmed and quality filtered using skewer v0.1.127[67] with the following
392 parameters (-q 20 -Q 20 -l 50 -n yes). Reads were then mapped to the *C. albicans* SC5314
393 genome (Assembly 21)[68] using BWA mem v0.7.15[69]. Duplicates were marked and read groups
394 added using the PICARD MarkDuplicates and AddOrReplaceReadGroups programs. Indels
395 were realigned using GATK 3.3 RealignerTargerCreator and IndelRealigner[70]. A set of high-
396 quality variants with variant scores of >100 were identified using GATK 3.3 HaplotypeCaller on
397 all samples simultaneously. These were then set as known sites when performing base quality
398 recalibration using GATK 3.3 PrintReads, AnalyzeCovariates and BaseRecalibrator to produce

bioRxiv preprint doi: https://doi.org/10.1101/2021.03.08.433668; this version posted March 8, 2021. The copyright holder for this preprint (which was not certified by peer review) is the author/funder, who has granted bioRxiv a license to display the preprint in perpetuity. It is made available under aCC-BY-NC-ND 4.0 International license.

399 finished bam files. GATK 3.3 HaplotypeCaller was then used again to call variants across
400 samples to produce a final vcf file. snpEff 4.2 was used to annotate variants using a custom
401 built database based on the *C. albicans* SC5314 genome (Assembly 21)[68].
402
403 **Transcriptome analysis**
404 RNA extraction, library preparations, and sequencing reactions were conducted at
405 GENEWIZ, LLC. (South Plainfield, NJ, USA). Total RNA was extracted from fresh frozen cell
406 pellets using Qiagen RNeasy Plus Universal mini kit following manufacturer's instruction
407 (Qiagen). Extracted RNA samples were quantified using Qubit 2.0 Fluorometer (Life
408 Technologies) and RNA integrity was checked using Agilent TapeStation 4200 (Agilent
409 Technologies). RNA sequencing libraries were prepared using the NEBNext Ultra II RNA
410 Library Prep Kit for Illumina following manufacturer's instructions (NEB). Briefly, mRNAs were
411 first enriched with Oligo(dT) beads. Enriched mRNAs were fragmented for 15 min at 94°C.
412 First strand and second strand cDNAs were subsequently synthesized. cDNA fragments were
413 end repaired and adenylated at 3' ends, and universal adapters were ligated to cDNA
414 fragments, followed by index addition and library enrichment by limited-cycle PCR. The
415 sequencing libraries were validated on the Agilent TapeStation (Agilent Technologies), and
416 quantified by using Qubit 2.0 Fluorometer (Invitrogen) as well as by quantitative PCR (KAPA
417 Biosystems). The sequencing libraries were pooled and clustered on 1 lane of a flowcell. After
418 clustering, the flowcell was loaded on the Illumina HiSeq instrument (4000 or equivalent)
419 according to manufacturer's instructions. The samples were sequenced using a 2 $\times$ 150bp
420 Paired End (PE) configuration. Image analysis and base calling were conducted by the HiSeq
421 Control Software (HCS). Raw sequence data (.bcl files) generated from Illumina HiSeq was
422 converted into fastq files and de-multiplexed using Illumina's bcl2fastq 2.17 software. One
423 mismatch was allowed for index sequence identification.

bioRxiv preprint doi: https://doi.org/10.1101/2021.03.08.433668; this version posted March 8, 2021. The copyright holder for this preprint (which was not certified by peer review) is the author/funder, who has granted bioRxiv a license to display the preprint in perpetuity. It is made available under aCC-BY-NC-ND 4.0 International license.

We performed quality profiling, adapter trimming, read filtering, and base correction for raw data using an all-in-one FASTQ preprocessor, *fastp*[71]. The high-quality paired-end reads were mapped to the *C. albicans* SC5314 genome (Assembly 22)[72] using HISAT2[73]. StringTie[74] was used to assemble the read alignments obtained in the previous step and estimate transcript abundances. Absolute mRNA abundance was expressed as fragments per kilobase of transcript per million mapped reads (FPKM). Differential expression analyses were conducted using DESeq2[75] package from Bioconductor[76] on R.

Western blotting

The fresh frozen cell pellets were lysed using the same volume of 2× SDS lysis buffer (5% SDS, 20% glycerol, 125 mM Tris-HCl, pH 6.8) supplemented with cOmplete EDTA-free protease inhibitor cocktail (Roche), 10 mM activated sodium orthovanadate, 2.5 mM sodium pyrophosphate, 1 mM β-glycerophosphate, 1% phosphatase inhibitor cocktail 2 (Millipore-Sigma), 1% phosphatase inhibitor cocktail 3 (Millipore-Sigma). Zirconia beads were added, and the cells were mechanically disrupted by 3 rounds of 1-min bead beating and 1-min cooling on ice. The samples were boiled at 95°C for 5 min. After centrifugation at 14,000 rpm for 5 min at 4°C to remove cellular debris, the supernatant was transferred to a new tube and this step was repeated. The protein concentration was measured using a BCA protein assay kit (Thermo Fisher Scientific). 2-Mercaptoethanol and bromophenol blue were added to 5% and 0.002% final concentration, respectively. The samples were boiled at 95°C for 5 min. Equal amounts of proteins were resolved by SDS-PAGE using the Mini-PROTEAN Tetra Cell system (Bio-Rad) and Tris/glycine/SDS running buffer. Subsequently, proteins were transferred to a nitrocellulose membrane (Amersham) using a semi-dry transfer apparatus. The membranes were blocked with 5% nonfat dry milk in TBS-T buffer (20 mM Tris-HCl, pH 7.6, 150 mM NaCl, 0.2% Tween-20) for 30 min and probed with CaBcy1 rabbit polyclonal antibody (GenScript) or CaTpk2 rabbit polyclonal antibody (GenScript), at 1:1,000 dilution in 5% nonfat dry milk in TBS-T buffer plus

bioRxiv preprint doi: https://doi.org/10.1101/2021.03.08.433668; this version posted March 8, 2021. The copyright holder for this preprint (which was not certified by peer review) is the author/funder, who has granted bioRxiv a license to display the preprint in perpetuity. It is made available under aCC-BY-NC-ND 4.0 International license.

0.5% sodium azide for 2 hours at room temperature. The membranes were then washed three times with TBS-T and incubated with an IRDye 800CW goat anti-rabbit IgG secondary antibody (LI-COR Biosciences) diluted at 1:10,000 in TBS-T. The membranes were washed three times with TBS-T, stored in TBS buffer, and visualized by scanning with an Odyssey CLx infrared imaging system (LI-COR Biosciences). For Coomassie stained gels, SDS-PAGE gels were performed as described and then stained in Coomassie Brilliant Blue solution (0.1% Coomassie R-250, 50% methanol, 40% water, 10% glacial acetic acid) overnight. Gels were incubated for 6 h in destaining solution (50% water, 40% methanol, 10% glacial acetic acid), rinsed with water, and analyzed by scanning with an Odyssey CLx infrared imaging system (LI-COR Biosciences). Resulting images were analyzed and quantified using ImageStudio software (LI-COR Biosciences).

Preparation of samples for mass spectrometry

The frozen cell pellet samples were processed by Tymora Analytical Operations (West Lafayette, IN). For lysis, 200 µL of lysis buffer (8M urea in 50mM Tris-Cl pH 7.5, supplemented with phosphatase inhibitor cocktail 3 [Millipore-Sigma]) was added to each of the pellets and pipetted up and down several time to lyse a portion of the pellet. The samples were incubated for 10 min at 37°C, pulse-sonicated several times with a sonicator probe, and incubated again for 10 min at 37°C. The lysed samples were then centrifuged at 16,000 g for 10 min to remove debris and the supernatant portions collected. BCA assay was carried out to calculate the protein concentration and all samples were normalized by protein amount to 200 µg each. Then 5 mM dithiothreitol was added and the proteins were incubated at 37°C for 15 min to reduce the cysteine residues, and then alkylated by incubation in 15 mM iodoacetamide at room temperature for 45 min in the dark. The samples were diluted 3-fold with 50 mM triethylammonium bicarbonate and digested with Lys-C (Wako) at 1:100 (w/w) enzyme-to-protein ratio for 3 h at 37°C. The samples were further diluted 3-fold with 50 mM

bioRxiv preprint doi: https://doi.org/10.1101/2021.03.08.433668; this version posted March 8, 2021. The copyright holder for this preprint (which was not certified by peer review) is the author/funder, who has granted bioRxiv a license to display the preprint in perpetuity. It is made available under aCC-BY-NC-ND 4.0 International license.

476 triethylammonium bicarbonate and trypsin was added to a final 1:50 (w/w) enzyme-to-protein
477 ratio for overnight digestion at 37°C. After digestion, the samples were acidified with
478 trifluoroacetic acid to a pH < 3 and desalted using Top-Tip C18 tips (Glygen) according to
479 manufacturer's instructions. A 1% portion of each sample was used for direct proteomics
480 analysis and the remainder of each sample was used for phosphopeptide enrichment. The
481 samples were dried completely in a vacuum centrifuge and stored at -80°C. The 99% portion of
482 each sample was used for phosphopeptides enrichment using PolyMAC Phosphopeptide
483 Enrichment Kit (Tymora Analytical) according to the manufacturer's instructions.
484
485 **Liquid chromatography with tandem mass spectrometry (LC-MS/MS) analysis**
486 The full phosphopeptide sample and 1 µg of the peptide sample each was dissolved in
487 10.5 µl of 0.05% trifluoroacetic acid with 3% (v/v) acetonitrile containing spiked-in indexed
488 Retention Time Standard artificially synthetized peptides (Biognosys). The spiked-in 11-
489 peptides standard mixture was used to account for any variation in retention times and to
490 normalize abundance levels among samples. Ten microliters of each sample was injected into
491 an Ultimate 3000 nano UHPLC system (Thermo Fisher Scientific). Peptides were captured on a
492 2-cm Acclaim PepMap trap column and separated on a heated 50-cm Acclaim PepMap column
493 (Thermo Fisher Scientific) containing C18 resin. The mobile phase buffer consisted of 0.1%
494 formic acid in ultrapure water (buffer A) with an eluting buffer of 0.1% formic acid in 80% (v/v)
495 acetonitrile (buffer B) run with a linear 90-min gradient of 6–30% buffer B at flow rate of 300
496 nL/min. The UHPLC was coupled online with a Q-Exactive HF-X mass spectrometer (Thermo
497 Fisher Scientific). The mass spectrometer was operated in the data-dependent mode, in which
498 a full-scan MS (from m/z 375 to 1,500 with the resolution of 60,000) was followed by MS/MS of
499 the 15 most intense ions (30,000 resolution; normalized collision energy - 28%; automatic gain
500 control target [AGC] - 2E4, maximum injection time - 200 ms; 60 sec exclusion).
501

bioRxiv preprint doi: https://doi.org/10.1101/2021.03.08.433668; this version posted March 8, 2021. The copyright holder for this preprint (which was not certified by peer review) is the author/funder, who has granted bioRxiv a license to display the preprint in perpetuity. It is made available under aCC-BY-NC-ND 4.0 International license.

LC-MS data processing

The raw files were searched directly against the *C. albicans* database updated in 2019 with no redundant entries, using Byonic (Protein Metrics) and Sequest search engines loaded into Proteome Discoverer 2.3 software (Thermo Fisher Scientific). MS1 precursor mass tolerance was set at 10 ppm, and MS2 tolerance was set at 20ppm. Search criteria included a static carbamidomethylation of cysteines (+57.0214 Da), and variable modifications of phosphorylation of S, T and Y residues (+79.996 Da), oxidation (+15.9949 Da) on methionine residues and acetylation (+42.011 Da) at N terminus of proteins. Search was performed with full trypsin/P digestion and allowed a maximum of two missed cleavages on the peptides analyzed from the sequence database. The false-discovery rates of proteins and peptides were set at 0.01. All protein and peptide identifications were grouped and any redundant entries were removed. Only unique peptides and unique master proteins were reported.

Label-free quantitation analysis

All data were quantified using the label-free quantitation node of Precursor Ions Quantifier through the Proteome Discoverer v2.3 (Thermo Fisher Scientific). For the quantification of proteomic and phosphoproteomic data, the intensities of peptides were extracted with initial precursor mass tolerance set at 10 ppm, minimum number of isotope peaks as 2, maximum ΔRT of isotope pattern multiplets – 0.2 min, PSM confidence FDR of 0.01, with hypothesis test of ANOVA, maximum RT shift of 5 min, pairwise ratio-based ratio calculation, and 100 as the maximum allowed fold change. The abundance levels of all peptides/phosphopeptides and proteins/phosphoproteins were normalized to the spiked-in internal iRT standard. For calculations of fold-change between the groups of proteins, total protein or phosphoprotein abundance values were added together and the ratios of these sums were used to compare proteins within different samples. When the protein abundance could not be determined, pseudo value (1) was given for logarithm.

bioRxiv preprint doi: https://doi.org/10.1101/2021.03.08.433668; this version posted March 8, 2021. The copyright holder for this preprint (which was not certified by peer review) is the author/funder, who has granted bioRxiv a license to display the preprint in perpetuity. It is made available under aCC-BY-NC-ND 4.0 International license.

528

529 **Phosphoproteomic data analysis**

530 Phosphopeptide abundance values were normalized by protein abundance values[77,78].
531 Fifteen-amino acid sequences around the phosphorylation site was extracted from the
532 phosphoproteome using a custom Microsoft Excel spreadsheet. rmotifx[79] package on R was
533 used to find overrepresented patterns from the 15-aa sequence set. Potential substrates of 6
534 kinases (Cdc28, PKA, Yck2, MAPK, Cbk1, and Gin4) were predicted from the
535 phosphoproteome based on their consensus phosphorylation motifs. The following consensus
536 motifs were retrieved from the Scansite 4.0 database[80]; Cdc28 ([S/T]-P-x-K/R); PKA (R/K-R/K-x-
537 [S/T]); Yck2 ([S/T]-x-x-[S/T]); MAPK (P-x-[S/T]-P); Cbk1 (H-x-K/R-x-x-[S/T] or H-x-x-K/R-x-
538 [S/T]); Gin4 (R-S-x-[S/T]). We next utilized a gene set enrichment analysis algorithm,
539 GSEA[46,81], to infer kinase activity based on the substrate phosphorylation levels from the
540 phosphoproteome.

541

542 **Data availability**

543 Requests for materials should be addressed to the corresponding author. The datasets
544 generated in this study can be found under NCBI BioProject PRJNA706677, including whole-
545 genome sequence data and RNA-seq data. Source data are provided with this paper.

546

547

bioRxiv preprint doi: https://doi.org/10.1101/2021.03.08.433668; this version posted March 8, 2021. The copyright holder for this preprint (which was not certified by peer review) is the author/funder, who has granted bioRxiv a license to display the preprint in perpetuity. It is made available under aCC-BY-NC-ND 4.0 International license.

REFERENCES

1. Min, K., Neiman, A.M. & Konopka, J.B. Fungal pathogens: Shape-shifting invaders. *Trends Microbiol.* **28**, 922-933 (2020).
2. Noble, S.M., Gianetti, B.A. & Witchley, J.N. *Candida albicans* cell-type switching and functional plasticity in the mammalian host. *Nat. Rev. Microbiol.* **15**, 96-108 (2017).
3. Sudbery, P.E. Growth of *Candida albicans* hyphae. *Nat. Rev. Microbiol.* **9**, 737-748 (2011).
4. da Silva Dantas, A. *et al.* Cell biology of *Candida albicans*-host interactions. *Curr. Opin. Microbiol.* **34**, 111-118 (2016).
5. Lu, Y., Su, C. & Liu, H. *Candida albicans* hyphal initiation and elongation. *Trends. Microbiol.* **22**, 707-714 (2014).
6. Naseem, S., Douglas, L.M. & Konopka, J.B. *Candida albicans rvs161Δ* and *rvs167Δ* endocytosis mutants are defective in invasion into the oral cavity. *mBio* **10**, e02503-19 (2019).
7. Biswas, S., Van Dijck, P. & Datta, A. Environmental sensing and signal transduction pathways regulating morphopathogenic determinants of *Candida albicans*. *Microbiol. Mol. Biol. Rev.* **71**, 348-376 (2007).
8. Min, K., Naseem, S. & Konopka, J.B. N-Acetylglucosamine regulates morphogenesis and virulence pathways in fungi. *J. Fungi (Basel)* **6**, 8 (2019).
9. Wang, Y. Fungal adenylyl cyclase acts as a signal sensor and integrator and plays a central role in interaction with bacteria. *PLoS Pathog.* **9**, e1003612 (2013).
10. Niimi, M. Dibutyryl cyclic AMP-enhanced germ tube formation in exponentially growing *Candida albicans* cells. *Fungal Genet. Biol.* **20**, 79-83 (1996).
11. Huang, G., Huang, Q., Wei, Y., Wang, Y. & Du, H. Multiple roles and diverse regulation of the Ras/cAMP/protein kinase A pathway in *Candida albicans*. *Mol. Microbiol.* **111**, 6-16 (2019).
12. Rocha, C.R. *et al.* Signaling through adenylyl cyclase is essential for hyphal growth and virulence in the pathogenic fungus *Candida albicans*. *Mol. Biol. Cell* **12**, 3631-3643 (2001).
13. Harcus, D., Nantel, A., Marcil, A., Rigby, T. & Whiteway, M. Transcription profiling of cyclic AMP signaling in *Candida albicans*. *Mol. Biol. Cell* **15**, 4490-4499 (2004).
14. Parrino, S.M. *et al.* cAMP-independent signal pathways stimulate hyphal morphogenesis in *Candida albicans*. *Mol. Microbiol.* **103**, 764-779 (2017).
15. Lu, Y., Su, C., Solis, N.V., Filler, S.G. & Liu, H. Synergistic regulation of hyphal elongation by hypoxia, CO_2, and nutrient conditions controls the virulence of *Candida albicans*. *Cell Host Microbe* **14**, 499-509 (2013).
16. Carlisle, P.L. *et al.* Expression levels of a filament-specific transcriptional regulator are sufficient to determine *Candida albicans* morphology and virulence. *Proc. Natl. Acad. Sci. U. S. A.* **106**, 599-604 (2009).
17. Bockmuhl, D.P. & Ernst, J.F. A potential phosphorylation site for an A-type kinase in the Efg1 regulator protein contributes to hyphal morphogenesis of *Candida albicans*. *Genetics* **157**, 1523-1530 (2001).
18. Lassak, T. *et al.* Target specificity of the *Candida albicans* Efg1 regulator. *Mol. Microbiol.* **82**, 602-618 (2011).
19. Martin, R. *et al.* A core filamentation response network in *Candida albicans* is restricted to eight genes. *PLoS One* **8**, e58613 (2013).
20. Naseem, S., Araya, E. & Konopka, J.B. Hyphal growth in *Candida albicans* does not require induction of hyphal-specific gene expression. *Mol. Biol. Cell* **26**, 1174-1187 (2015).

bioRxiv preprint doi: https://doi.org/10.1101/2021.03.08.433668; this version posted March 8, 2021. The copyright holder for this preprint (which was not certified by peer review) is the author/funder, who has granted bioRxiv a license to display the preprint in perpetuity. It is made available under aCC-BY-NC-ND 4.0 International license.

21. Giusani, A.D., Vinces, M. & Kumamoto, C.A. Invasive filamentous growth of *Candida albicans* is promoted by Czf1p-dependent relief of Efg1p-mediated repression. *Genetics* **160**, 1749-1753 (2002).
22. Woolford, C.A. *et al.* Bypass of *Candida albicans* filamentation/biofilm regulators through diminished expression of protein kinase Cak1. *PLoS Genet.* **12**, e1006487 (2016).
23. Rai, L.S. *et al.* The *Candida albicans* biofilm gene circuit modulated at the chromatin level by a recent molecular histone innovation. *PLoS Biol.* **17**, e3000422 (2019).
24. Wang, Y. Hgc1-Cdc28-how much does a single protein kinase do in the regulation of hyphal development in *Candida albicans*? *J. Microbiol.* **54**, 170-177 (2016).
25. Zheng, X.D., Lee, R.T., Wang, Y.M., Lin, Q.S. & Wang, Y. Phosphorylation of Rga2, a Cdc42 GAP, by CDK/Hgc1 is crucial for *Candida albicans* hyphal growth. *EMBO J.* **26**, 3760-3769 (2007).
26. Bishop, A. *et al.* Hyphal growth in *Candida albicans* requires the phosphorylation of Sec2 by the Cdc28-Ccn1/Hgc1 kinase. *EMBO J.* **29**, 2930-2942 (2010).
27. Caballero-Lima, D. & Sudbery, P.E. In *Candida albicans*, phosphorylation of Exo84 by Cdk1-Hgc1 is necessary for efficient hyphal extension. *Mol. Biol. Cell.* **25**, 1097-1110 (2014).
28. Sinha, I. *et al.* Cyclin-dependent kinases control septin phosphorylation in *Candida albicans* hyphal development. *Dev. Cell.* **13**, 421-432 (2007).
29. Zeng, G., Wang, Y.M. & Wang, Y. Cdc28-Cln3 phosphorylation of Sla1 regulates actin patch dynamics in different modes of fungal growth. *Mol. Biol. Cell* **23**, 3485-3497 (2012).
30. Gutierrez-Escribano, P. *et al.* CDK-dependent phosphorylation of Mob2 is essential for hyphal development in *Candida albicans*. *Mol. Biol. Cell* **22**, 2458-2469 (2011).
31. Gonzalez-Novo, A. *et al.* Sep7 is essential to modify septin ring dynamics and inhibit cell separation during *Candida albicans* hyphal growth. *Mol. Biol. Cell* **19**, 1509-1518 (2008).
32. Wang, A., Raniga, P.P., Lane, S., Lu, Y. & Liu, H. Hyphal chain formation in *Candida albicans*: Cdc28-Hgc1 phosphorylation of Efg1 represses cell separation genes. *Mol. Cell Biol.* **29**, 4406-4416 (2009).
33. Matsumoto, K., Uno, I., Oshima, Y. & Ishikawa, T. Isolation and characterization of yeast mutants deficient in adenylate cyclase and cAMP-dependent protein kinase. *Proc. Natl. Acad. Sci. U. S. A.* **79**, 2355-2359 (1982).
34. McEachern, M.J. & Hicks, J.B. Unusually large telomeric repeats in the yeast *Candida albicans*. *Mol. Cell. Biol.* **13**, 551-560 (1993).
35. Todd, R.T., Wikoff, T.D., Forche, A. & Selmecki, A. Genome plasticity in *Candida albicans* is driven by long repeat sequences. *Elife* **8**, e45954 (2019).
36. Andaluz, E. *et al.* Rad52 function prevents chromosome loss and truncation in *Candida albicans*. *Mol. Microbiol.* **79**, 1462-1482 (2011).
37. Pennaneach, V., Putnam, C.D. & Kolodner, R.D. Chromosome healing by de novo telomere addition in *Saccharomyces cerevisiae*. *Mol. Microbiol.* **59**, 1357-1368 (2006).
38. Legrand, M., Jaitly, P., Feri, A., d'Enfert, C. & Sanyal, K. *Candida albicans*: an emerging yeast model to study eukaryotic genome plasticity. *Trends. Genet.* **35**, 292-307 (2019).
39. Min, K., Ichikawa, Y., Woolford, C.A. & Mitchell, A.P. *Candida albicans* gene deletion with a transient CRISPR-Cas9 system. *mSphere* **1**, e00130-16 (2016).
40. Reuss, O., Vik, A., Kolter, R. & Morschhauser, J. The *SAT1* flipper, an optimized tool for gene disruption in *Candida albicans*. *Gene* **341**, 119-127 (2004).
41. Willger, S.D. *et al.* Analysis of the *Candida albicans* Phosphoproteome. *Eukaryot. Cell* **14**, 474-485 (2015).
42. Su, C., Lu, Y. & Liu, H. N-acetylglucosamine sensing by a GCN5-related *N*-acetyltransferase induces transcription via chromatin histone acetylation in fungi. *Nat. Commun.* **7**, 12916 (2016).

bioRxiv preprint doi: https://doi.org/10.1101/2021.03.08.433668; this version posted March 8, 2021. The copyright holder for this preprint (which was not certified by peer review) is the author/funder, who has granted bioRxiv a license to display the preprint in perpetuity. It is made available under aCC-BY-NC-ND 4.0 International license.

43. Naseem, S., Gunasekera, A., Araya, E. & Konopka, J.B. N-Acetylglucosamine (GlcNAc) induction of hyphal morphogenesis and transcriptional responses in *Candida albicans* are not dependent on its metabolism. *J. Biol. Chem.* **286**, 28671-28680 (2011).
44. Cao, C. *et al.* Global regulatory roles of the cAMP/PKA pathway revealed by phenotypic, transcriptomic and phosphoproteomic analyses in a null mutant of the PKA catalytic subunit in *Candida albicans*. *Mol. Microbiol.* **105**, 46-64 (2017).
45. Frazer, C. *et al.* Epigenetic cell fate in *Candida albicans* is controlled by transcription factor condensates acting at super-enhancer-like elements. *Nature Microbiol.* **5**, 1374-1389 (2020).
46. Subramanian, A. *et al.* Gene set enrichment analysis: a knowledge-based approach for interpreting genome-wide expression profiles. *Proc. Natl. Acad. Sci. U. S. A.* **102**, 15545-15550 (2005).
47. Greig, J.A. *et al.* Cell cycle-independent phospho-regulation of Fkh2 during hyphal growth regulates *Candida albicans* pathogenesis. *PLoS Pathog.* **11**, e1004630 (2015).
48. Blankenship, J.R., Fanning, S., Hamaker, J.J. & Mitchell, A.P. An extensive circuitry for cell wall regulation in *Candida albicans*. *PLoS Pathog.* **6**, e1000752 (2010).
49. Jung, S.I. *et al.* Yeast casein kinase 2 governs morphology, biofilm formation, cell wall integrity, and host cell damage of *Candida albicans*. *PLoS One* **12**, e0187721 (2017).
50. Caplan, T. *et al.* Overcoming fungal echinocandin resistance through inhibition of the non-essential stress kinase Yck2. *Cell Chem. Biol.* **27**, 269-282 (2020).
51. Li, C.R. *et al.* The formin family protein CaBni1p has a role in cell polarity control during both yeast and hyphal growth in *Candida albicans*. *J. Cell Sci.* **118**, 2637-2648 (2005).
52. Buccitelli, C. & Selbach, M. mRNAs, proteins and the emerging principles of gene expression control. *Nat. Rev. Genet.* **21**, 630-644 (2020).
53. Carlisle, P.L. & Kadosh, D. *Candida albicans* Ume6, a filament-specific transcriptional regulator, directs hyphal growth via a pathway involving Hgc1 cyclin-related protein. *Eukaryot. Cell* **9**, 1320-1328 (2010).
54. Khajuria, R.K. *et al.* Ribosome levels selectively regulate translation and lineage commitment in human hematopoiesis. *Cell* **173**, 90-103 (2018).
55. Desai, P.R. *et al.* The 5' untranslated region of the *EFG1* transcript promotes its translation to regulate hyphal morphogenesis in *Candida albicans*. *mSphere* **3**, e00280-18 (2018).
56. Hossain, S., Lash, E., Veri, A.O. & Cowen, L.E. Functional connections between cell cycle and proteostasis in the regulation of *Candida albicans* morphogenesis. *Cell Reports* **34**, 108781 (2021).
57. Lu, Y., Su, C., Ray, S., Yuan, Y. & Liu, H. CO2 signaling through the Ptc2-Ssn3 axis governs sustained hyphal development of *Candida albicans* by reducing Ume6 phosphorylation and degradation. *mBio* **10**, e02320-18 (2019).
58. Bai, C. *et al.* Characterization of a hyperactive Cyr1 mutant reveals new regulatory mechanisms for cellular cAMP levels in *Candida albicans*. *Mol. Microbiol.* **82**, 879-893 (2011).
59. Selmecki, A., Forche, A. & Berman, J. Aneuploidy and isochromosome formation in drug-resistant *Candida albicans*. *Science* **313**, 367-370 (2006).
60. Todd, R.T. & Selmecki, A. Expandable and reversible copy number amplification drives rapid adaptation to antifungal drugs. *Elife* **9**, e58349 (2020).
61. Kebaara, B.W. *et al. Candida albicans* Tup1 is involved in farnesol-mediated inhibition of filamentous-growth induction. *Eukaryot. Cell* **7**, 980-987 (2008).
62. Marton, T., Maufrais, C., d'Enfert, C. & Legrand, M. Use of CRISPR-Cas9 to target homologous recombination limits transformation-induced genomic changes in *Candida albicans*. *mSphere* **5**, e00620-20 (2020).

bioRxiv preprint doi: https://doi.org/10.1101/2021.03.08.433668; this version posted March 8, 2021. The copyright holder for this preprint (which was not certified by peer review) is the author/funder, who has granted bioRxiv a license to display the preprint in perpetuity. It is made available under aCC-BY-NC-ND 4.0 International license.

63. Min, K., Biermann, A., Hogan, D.A. & Konopka, J.B. Genetic analysis of *NDT80* family transcription factors in *Candida albicans* using new CRISPR-Cas9 approaches. *mSphere* **3**, e00545-18 (2018).
64. Vyas, V.K., Barrasa, M.I. & Fink, G.R. A *Candida albicans* CRISPR system permits genetic engineering of essential genes and gene families. *Sci. Adv.* **1**, e1500248 (2015).
65. Vyas, V.K. *et al.* New CRISPR mutagenesis strategies reveal variation in repair mechanisms among fungi. *mSphere* **3**, e00154-18 (2018).
66. De Backer, M.D. *et al.* Transformation of *Candida albicans* by electroporation. *Yeast* **15**, 1609-1618 (1999).
67. Jiang, H., Lei, R., Ding, S.W. & Zhu, S. Skewer: a fast and accurate adapter trimmer for next-generation sequencing paired-end reads. *BMC Bioinformatics* **15**, 182 (2014).
68. Skrzypek, M.S.B., J.; Binkley, G.; Miyasato, S.R.; Simison, M.; Sherlock, G. Candida Genome Database. Vol. 2017 (2017).
69. Li, H. & Durbin, R. Fast and accurate long-read alignment with Burrows-Wheeler transform. *Bioinformatics* **26**, 589-595 (2010).
70. DePristo, M.A. *et al.* A framework for variation discovery and genotyping using next-generation DNA sequencing data. *Nat. Genet.* **43**, 491-498 (2011).
71. Chen, S., Zhou, Y., Chen, Y. & Gu, J. fastp: an ultra-fast all-in-one FASTQ preprocessor. *Bioinformatics* **34**, i884-i890 (2018).
72. Skrzypek, M.S. *et al.* The Candida Genome Database (CGD): incorporation of Assembly 22, systematic identifiers and visualization of high throughput sequencing data. *Nucleic Acids Res.* **45**, D592-D596 (2017).
73. Kim, D., Langmead, B. & Salzberg, S.L. HISAT: a fast spliced aligner with low memory requirements. *Nat. Methods* **12**, 357-360 (2015).
74. Pertea, M., Kim, D., Pertea, G.M., Leek, J.T. & Salzberg, S.L. Transcript-level expression analysis of RNA-seq experiments with HISAT, StringTie and Ballgown. *Nat. Protoc.* **11**, 1650-1667 (2016).
75. Love, M.I., Huber, W. & Anders, S. Moderated estimation of fold change and dispersion for RNA-seq data with DESeq2. *Genome Biol.* **15**, 550 (2014).
76. Gentleman, R.C. *et al.* Bioconductor: open software development for computational biology and bioinformatics. *Genome Biol.* **5**, R80 (2004).
77. Wu, R. *et al.* Correct interpretation of comprehensive phosphorylation dynamics requires normalization by protein expression changes. *Mol. Cell. Proteomics* **10**, M111.009654 (2011).
78. Tan, H. *et al.* Integrative proteomics and phosphoproteomics profiling reveals dynamic signaling networks and bioenergetics pathways underlying T cell activation. *Immunity* **46**, 488-503 (2017).
79. Wagih, O., Sugiyama, N., Ishihama, Y. & Beltrao, P. Uncovering phosphorylation-based specificities through functional interaction networks. *Mol. Cell Proteomics* **15**, 236-245 (2016).
80. Obenauer, J.C., Cantley, L.C. & Yaffe, M.B. Scansite 2.0: Proteome-wide prediction of cell signaling interactions using short sequence motifs. *Nucleic Acids Res.* **31**, 3635-3641 (2003).
81. Mootha, V.K. *et al.* PGC-1alpha-responsive genes involved in oxidative phosphorylation are coordinately downregulated in human diabetes. *Nat. Genet.* **34**, 267-273 (2003).
82. Abbey, D.A. *et al.* YMAP: a pipeline for visualization of copy number variation and loss of heterozygosity in eukaryotic pathogens. *Genome Med.* **6**, 100 (2014).
83. Baum, K., Schuchhardt, J., Wolf, J. & Busse, D. Of gene expression and cell division time: A mathematical framework for advanced differential gene expression and data analysis. *Cell Syst.* **9**, 569-579 e7 (2019).

bioRxiv preprint doi: https://doi.org/10.1101/2021.03.08.433668; this version posted March 8, 2021. The copyright holder for this preprint (which was not certified by peer review) is the author/funder, who has granted bioRxiv a license to display the preprint in perpetuity. It is made available under aCC-BY-NC-ND 4.0 International license.

ACKNOWLEDGEMENTS

This work was supported by Public Health Service grants from the National Institutes of Health awarded to J.B.K. (R01GM116048 and R01AI047837). We thank Jihye An for help with microscopic image analysis and the members of our laboratories for their helpful comments on the manuscript.

AUTHOR CONTRIBUTIONS

K.M. and J.B.K conceived the study. K.M., T.F.J., H.S., K.R.V., J.D.H., and J.B.K. investigated the study. K.M., K.R.V., and J.D.H. formally analyzed the study. K.M. and J.B.K. wrote the original draft of the manuscript. K.M., T.F.J., H.S., K.R.V., J.D.H., and J.B.K reviewed and edited the manuscript. J.B.K supervised the study.

COMPETING INTERESTS STATEMENT

The authors declare no competing interests.

Table 1. Phenotypic and genetic variations of *cyr1*Δ/Δ pseudorevertants (PRs)

Strain	PR class	Doubling time (h)[†]	Filamentation (%)[‡]	Short genotype[§]
WT		1.4 ± 0.07	98 ± 2.3	Prototrophic wild type strain
*cyr1*Δ/Δ		3.4 ± 0.36[b]	0[b]	*cyr1*Δ/Δ (parental strain)
PR13, PR19	Class 1	1.5 ± 0.19	74 ± 4.4[b]	*bcy1*/BCY1 cyr1*Δ/Δ
PR12, PR14	Class 2	1.8 ± 0.09[a]	93 ± 2.3	Monosomy of ~276 kb of Chr2L; *cyr1*Δ/Δ
PR18	Class 3	2.3 ± 0.06[b]	93 ± 4.2	Monosomy of ~590 kb of Chr2L; *cyr1*Δ/Δ
PR16	Class 3+	2.4 ± 0.18[b]	82 ± 16.4[a]	Monosomy of ~557 kb of Chr2L; trisomy of ~1.3 Mb of Chr2; *cyr1*Δ/Δ

[†] Doubling times were measured in liquid YPD medium at 30°C. Shown is the mean ± SD of 4 independent experiments.

[‡] The percent of filamentous cells was measured 3 h after growth in GlcNAc medium at 37°C. Shown is the mean ± SD of at least 3 independent experiments with at least 100 cells counted for each condition.

[†‡] The p-value was calculated using one-way ANOVA with Dunnett's multiple comparisons test comparing the strains with the WT control; [a] $p < 0.01$, [b] $p < 0.0001$.

[§] An asterisk indicates a nonsense mutation. Chr2L, left arm of chromosome 2.

bioRxiv preprint doi: https://doi.org/10.1101/2021.03.08.433668; this version posted March 8, 2021. The copyright holder for this preprint (which was not certified by peer review) is the author/funder, who has granted bioRxiv a license to display the preprint in perpetuity. It is made available under aCC-BY-NC-ND 4.0 International license.

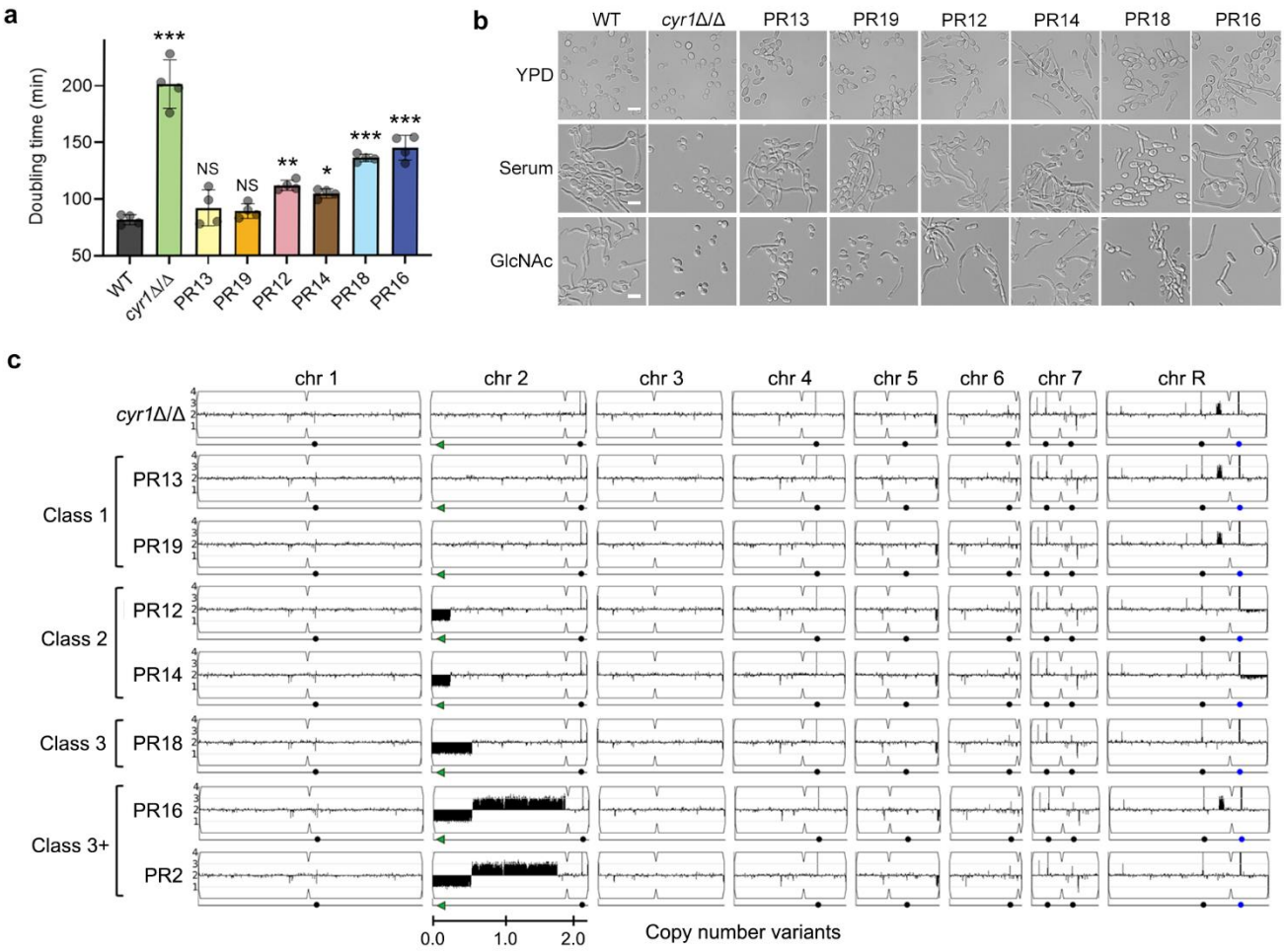

Fig. 1. Genetic changes in chromosome 2 bypassed the need for cAMP to improve growth and hyphal induction in *cyr1*Δ/Δ PR mutants.

a, Doubling times were measured in liquid YPD medium at 30°C. Shown is the mean ± SD (standard deviation) of 4 independent experiments. Statistical analysis was performed using one-way ANOVA with Dunnett's multiple comparisons test comparing the strains with the wild-type control (WT); ^{NS} $p > 0.05$, * $p < 0.05$, ** $p < 0.01$, *** $p < 0.001$.

b, The strains indicated at the top were grown in the liquid medium indicated on the left, and then hyphal induction was assessed microscopically. Cells were grown in liquid medium containing 15% serum or 50 mM N-acetylglucosamine (GlcNAc) to induce hyphal growth. Cells were incubated at 37°C for 3 h and then photographed. Scale bar, 10 μm.

bioRxiv preprint doi: https://doi.org/10.1101/2021.03.08.433668; this version posted March 8, 2021. The copyright holder for this preprint (which was not certified by peer review) is the author/funder, who has granted bioRxiv a license to display the preprint in perpetuity. It is made available under aCC-BY-NC-ND 4.0 International license.

788 **c**, Copy number variation analysis based upon read depth across the genome. Copy number estimates
789 scaled to genome ploidy (Y-axis) and chromosome location (X-axis) were plotted using YMAP[82].
790 Numbers and symbols below chromosomes indicate chromosomal position (Mb), *BCY1* gene (green
791 arrows), centromere locus (indentations in the chromosome cartoon), major repeat sequence position
792 (black circles), and rDNA locus (blue circles, ChrR).
793

bioRxiv preprint doi: https://doi.org/10.1101/2021.03.08.433668; this version posted March 8, 2021. The copyright holder for this preprint (which was not certified by peer review) is the author/funder, who has granted bioRxiv a license to display the preprint in perpetuity. It is made available under aCC-BY-NC-ND 4.0 International license.

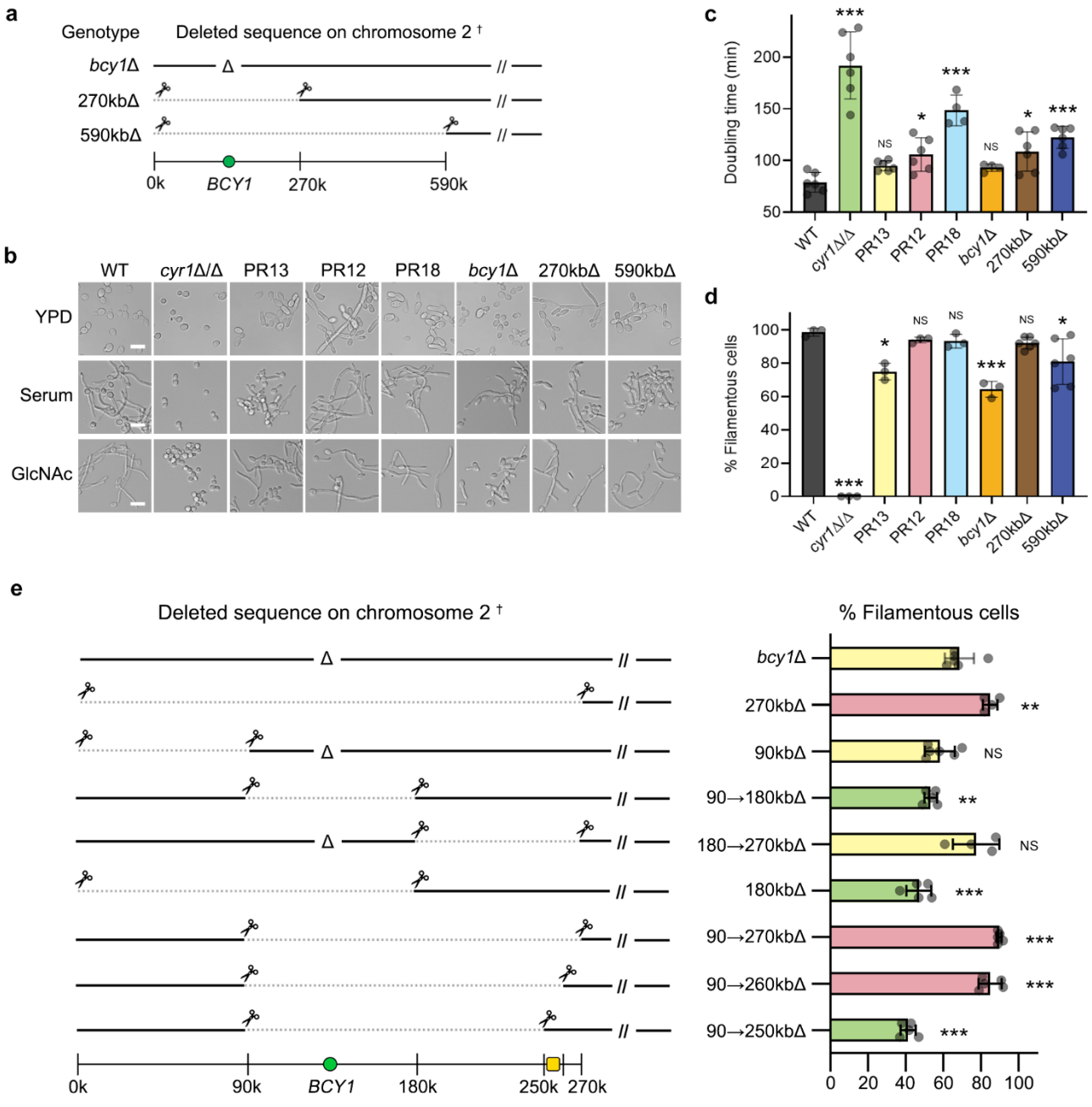

Fig. 2. Gene mapping by CRISPR-Cas9 demonstrates that haploinsufficiency of genes in chromosome 2 improved hyphal induction in *cyr1*Δ/Δ PR mutants.

a, A schematic diagram showing deleted sequences on chromosome 2.

b, The strains indicated at the top were grown in the liquid medium indicated on the left, and then hyphal induction was assessed microscopically. Cells were grown in liquid medium containing 15%

bioRxiv preprint doi: https://doi.org/10.1101/2021.03.08.433668; this version posted March 8, 2021. The copyright holder for this preprint (which was not certified by peer review) is the author/funder, who has granted bioRxiv a license to display the preprint in perpetuity. It is made available under aCC-BY-NC-ND 4.0 International license.

serum or 50 mM GlcNAc to induce hyphal growth at 37°C for 3 h and then photographed. Scale bar, 10 μm.

c, Doubling times were measured in liquid YPD medium at 30°C. Shown is the mean ± SD of 6 independent experiments.

d, Graph indicating the percent of filamentous cells after growth in GlcNAc medium described in panel **b**. Shown is the mean ± SD of at least 3 independent experiments with at least 100 cells counted for each condition.

e, Gene mapping by CRISPR-Cas9 identified a 10-kb region (yellow square) that is involved in the filamentous phenotype. The left panel shows deleted sequences on chromosome 2. The right panel shows the percent of filamentous cells in liquid GlcNAc medium at 37°C; green, weak hyphal induction; yellow, intermediate hyphal induction; pink, strong hyphal induction.

a,**e**, † Note that deletions are heterozygous; the cells retain a wild type version of chromosome 2. Numbers and symbols indicate gene deletion (Δ), CRISPR cut site (scissors), large genomic deletion (dotted line), *BCY1* gene (green circles), and chromosomal position (kb).

c,**d**,**e** Statistical analysis was performed using one-way ANOVA with Dunnett's multiple comparisons test comparing the strains with the WT or parental strain; ^{NS} $p > 0.05$, * $p < 0.05$, ** $p < 0.01$, *** $p < 0.001$.

bioRxiv preprint doi: https://doi.org/10.1101/2021.03.08.433668; this version posted March 8, 2021. The copyright holder for this preprint (which was not certified by peer review) is the author/funder, who has granted bioRxiv a license to display the preprint in perpetuity. It is made available under aCC-BY-NC-ND 4.0 International license.

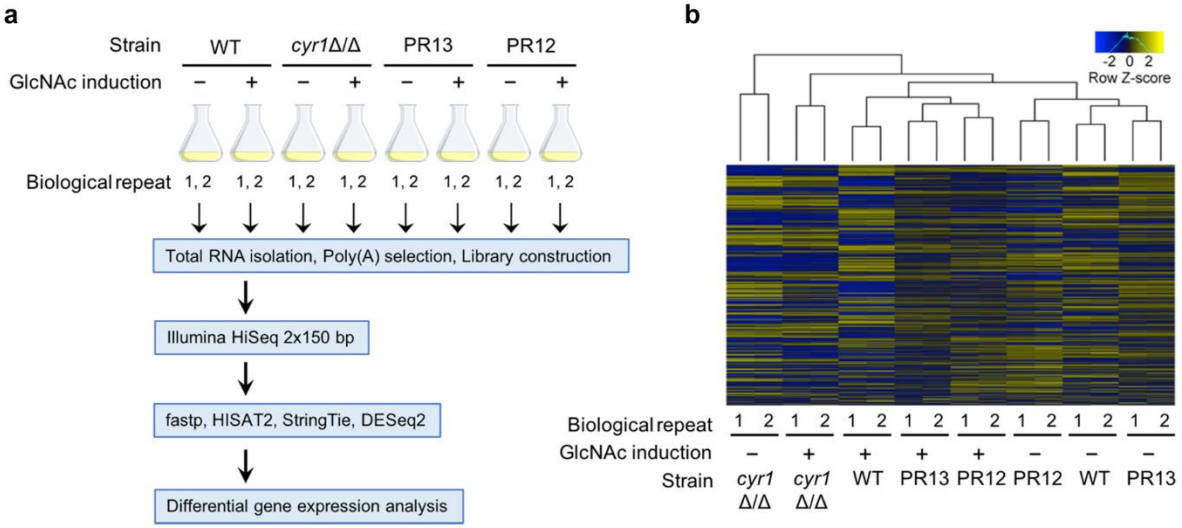

c

GlcNAc	WT −	WT +	*cyr1*Δ/Δ −	*cyr1*Δ/Δ +	PR13 −	PR13 +	PR12 −	PR12 +	
NAG1	0.0	5.8	-0.4	5.6	-0.3	5.8	0.2	5.6	GlcNAc catabolic genes
NGT1	0.0	5.6	-0.3	5.9	0.1	6.1	0.3	5.3	
DAC1	0.0	5.5	-0.2	5.4	-0.1	5.4	0.3	5.2	
HXK1	0.0	4.4	0.2	4.4	-0.2	4.3	-0.3	4.1	
ECE1	0.0	4.9	-4.9	-4.7	0.1	4.5	2.9	4.8	Hyphae-specific genes
HWP1	0.0	3.2	-5.8	-5.1	0.2	3.4	3.0	4.2	
HYR1	0.0	2.7	-1.9	-3.0	-0.8	2.0	2.0	2.5	
ALS3	0.0	1.7	-2.0	-1.8	-0.6	0.9	-0.1	1.3	
HGC1	0.0	1.6	-0.1	0.2	1.0	1.8	0.4	1.6	
UME6	0.0	1.4	-4.4	-5.0	-1.2	0.6	-0.4	0.6	Hyphal regulator transcription factors
BRG1	0.0	1.1	0.3	-0.2	0.9	0.6	0.6	1.1	
BCR1	0.0	0.4	0.7	1.0	0.2	0.6	-0.5	0.2	
EFG1	0.0	0.2	0.3	-0.2	0.1	0.2	-0.4	-0.2	
NDT80	0.0	-0.1	-0.5	-0.4	0.1	-0.3	-1.4	-1.1	
CYR1	0.0	0.2	-10.2	-9.4	-16.3	-12.3	-11.7	-9.9	cAMP-PKA pathway genes
BCY1	0.0	0.1	0.5	0.3	-0.2	-0.4	-1.1	-0.9	
TPK1	0.0	-0.2	-0.6	-0.5	-0.1	-0.2	-0.1	-0.1	
TPK2	0.0	-0.3	1.2	0.9	0.6	0.3	0.2	0.3	
ACT1	0.0	0.3	0.2	0.2	0.1	0.2	-0.2	0.2	Housekeeping genes
TEF1	0.0	-0.2	-0.2	-0.3	0.0	-0.3	-0.5	-0.5	

Fig. 3. cAMP signaling is not necessary in transcriptional regulation of the genes during hyphal induction.

a, Experimental scheme of transcriptomic analysis. Cells were grown at 37°C in liquid galactose medium and then 50 mM GlcNAc was added for 2 h to induce hyphae.

b, Cluster analysis of differentially expressed genes (DEGs).

bioRxiv preprint doi: https://doi.org/10.1101/2021.03.08.433668; this version posted March 8, 2021. The copyright holder for this preprint (which was not certified by peer review) is the author/funder, who has granted bioRxiv a license to display the preprint in perpetuity. It is made available under aCC-BY-NC-ND 4.0 International license.

825 **c**, Summary of differential expression analysis. The numbers in colored boxes are $\log_2$ difference of
826 transcript levels compared to the wild-type −GlcNAc condition. Grey boxes indicate the difference is
827 not significantly different (adjusted $p > 0.1$).
828

bioRxiv preprint doi: https://doi.org/10.1101/2021.03.08.433668; this version posted March 8, 2021. The copyright holder for this preprint (which was not certified by peer review) is the author/funder, who has granted bioRxiv a license to display the preprint in perpetuity. It is made available under aCC-BY-NC-ND 4.0 International license.

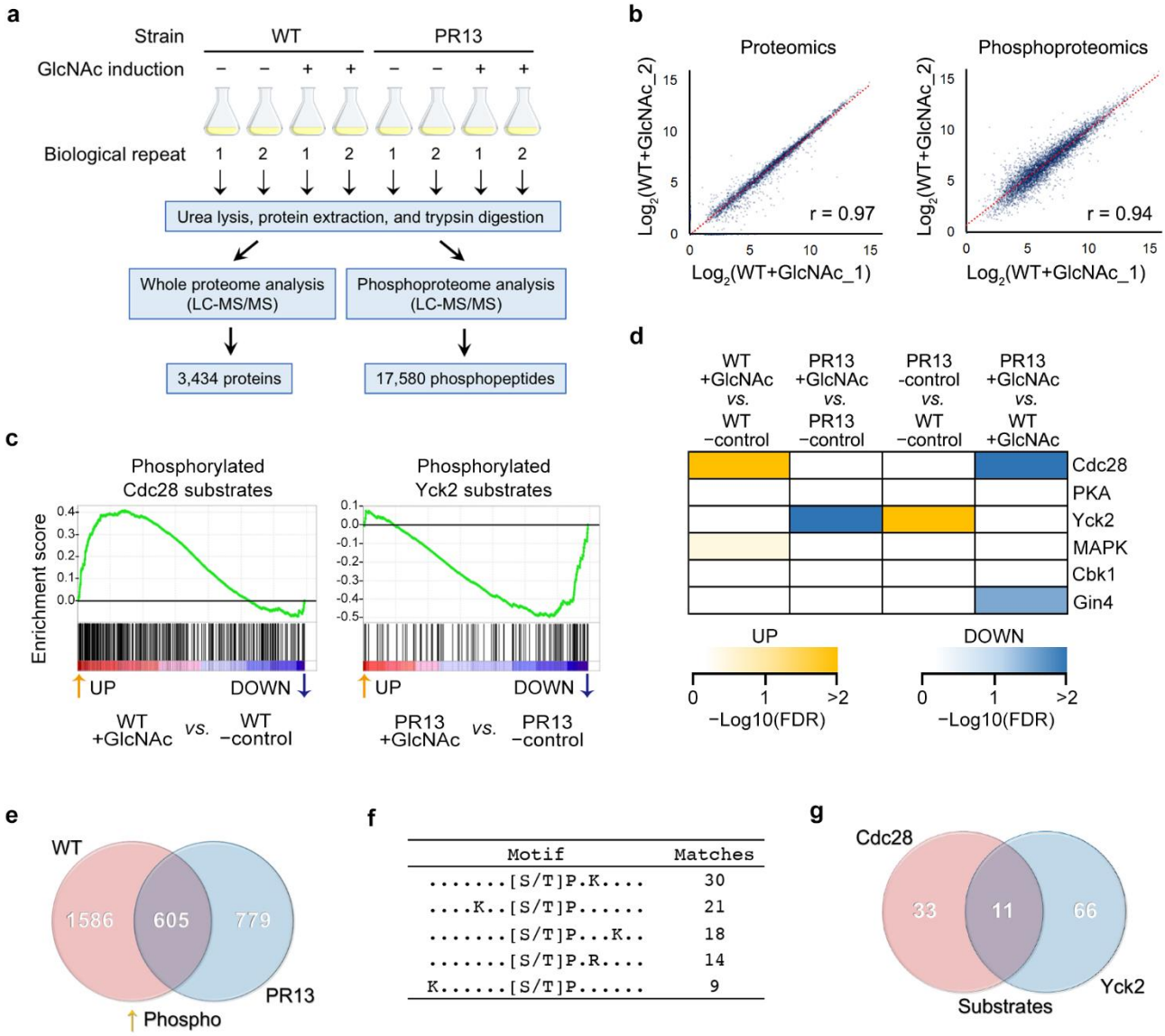

Fig. 4. Quantitative phosphoproteomics detected activity of two key kinases in hyphal induction.

a, Experimental scheme of parallel proteomic and phosphoproteomic analyses. Cells were grown at 37°C in liquid galactose medium and then 50 mM GlcNAc was added for 2 h to induce hyphae. For phosphorylation analysis, phosphopeptides were enriched by polymer-based metal-ion affinity capture (PolyMAC).

bioRxiv preprint doi: https://doi.org/10.1101/2021.03.08.433668; this version posted March 8, 2021. The copyright holder for this preprint (which was not certified by peer review) is the author/funder, who has granted bioRxiv a license to display the preprint in perpetuity. It is made available under aCC-BY-NC-ND 4.0 International license.

b, Representative null comparisons of the biological replicates show high reproducibility. We compared the replicate data of WT+GlcNAc_1 and WT+GlcNAc_2 from both whole proteome and phosphoproteome.

c, Representative results of kinase-substrate enrichment analysis. Gene set enrichment analysis (GSEA) algorithm[46] was used to identify significantly enriched or depleted groups of phosphorylated substrates.

d, The color-coded diagram illustrates changes of the selected kinase activities indicated by the scale bar at the bottom (< 25% false discovery rate [FDR]). Kinase activity inference was based on the collective phosphorylation changes of their identified substrates.

e, Venn diagrams of phosphopeptides upregulated during hyphal induction ($\log_2$ fold change > 0.5). Note that 605 phosphopeptides were upregulated in both WT and PR13 strains.

f, Overrepresented motifs were extracted from the 605 phosphopeptides, using the motif-x algorithm[79] ($p < 10^{-6}$). 44 phosphopeptides had the Cdc28 consensus motif ([S/T]-P-x-K/R) indicating they were potential substrates.

g, Venn diagrams of the upregulated Cdc28 substrates ([S/T]-P-x-K/R) or Yck2 substrates (S/T-x-x-[S/T]). 11 phosphopeptides were potential substrates of both Cdc28 and Yck2 kinases.

bioRxiv preprint doi: https://doi.org/10.1101/2021.03.08.433668; this version posted March 8, 2021. The copyright holder for this preprint (which was not certified by peer review) is the author/funder, who has granted bioRxiv a license to display the preprint in perpetuity. It is made available under aCC-BY-NC-ND 4.0 International license.

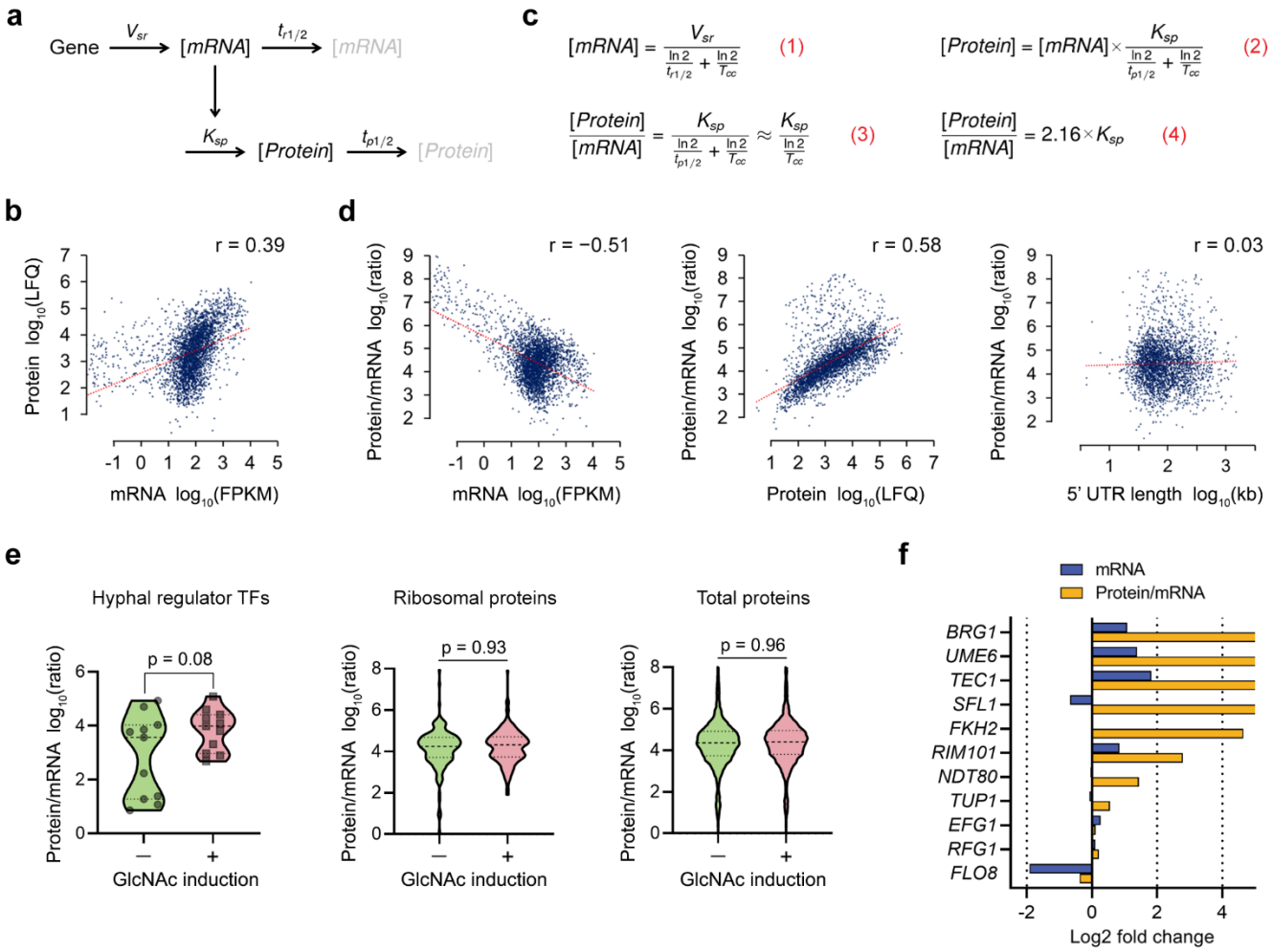

Fig. 5. Integrated transcriptomic and proteomic analyses indicate that hyphal stimulation induces translation of hyphal regulator TFs.

a, A basic gene expression model with key parameters (adopted from REF.[52,83]). The mRNA is transcribed with rate V_{sr} and degraded with a half-life represented by $t_{r1/2}$. The protein is translated proportionally to the mRNA abundance with the rate constant K_{sp} and degraded with a half-life of $t_{p1/2}$. **b**, An across-gene correlation analysis comparing estimates of absolute mRNA abundance (expressed in fragments per kilobase of transcript per million mapped reads (FPKM)) to protein abundance (expressed as label free quantitation (LFQ)) in exponentially growing WT cells. r, Pearson correlation coefficient.

bioRxiv preprint doi: https://doi.org/10.1101/2021.03.08.433668; this version posted March 8, 2021. The copyright holder for this preprint (which was not certified by peer review) is the author/funder, who has granted bioRxiv a license to display the preprint in perpetuity. It is made available under aCC-BY-NC-ND 4.0 International license.

c, Mathematical expression of mRNA (Equation 1) and protein abundances (Equation 2) as a function of key gene expression parameters, including cell doubling time T_{cc}, as detailed in REF.[83]. Rearranging Equation 2 yields the dependency of protein-mRNA abundance ratio on the translation rate constant K_{sp}, cell doubling time T_{cc}, and protein half-life $t_{p1/2}$ (Equation 3). We neglected protein degradation assuming that protein replacement is generally driven by dilution due to cell division in exponentially growing *C. albicans* cells ($t_{p1/2} >> T_{cc}$). Substituting the cell doubling time (T_{cc} = 1.5 h in *C. albicans*) yields Equation 4. Therefore, we can approximate the translation rate with the protein-to-mRNA level ratio.

d, Across-gene correlation analyses comparing protein-to-mRNA ratio versus mRNA abundance, protein abundance, and 5' UTR length (from left to right). r, Pearson correlation coefficient.

e, Protein-to-mRNA ratios of 11 selected hyphal regulator transcription factors (TFs) during GlcNAc induction. The protein-to-mRNA ratios of the 5 hyphal regulators were two orders of magnitude lower than the median in −GlcNAc control, indicating their translation rate was very low before hyphal induction. The p-value was calculated using two-sided unpaired t-test (hyphal regulator TFs) and z-test (ribosomal proteins and total proteins).

f, The relative change in protein-to-mRNA ratio for the selected 11 hyphal regulators is shown in yellow, relative changes in mRNA expression are shown in blue. The protein-to-mRNA ratio of *UME6*, *SFL1*, *BRG1*, *TEC1*, and *FKH2* increased dramatically (log2 fold change > 4) during hyphal induction while mRNA levels did not.

Extended Data Table 1. Genome analysis summary

Strain	PR Class	Short genotype	*de novo* telomere addition†	Telomere seed sequence
*cyr1*Δ/Δ	-	*cyr1*Δ/Δ	-	-
PR13	1	*bcy1-Q82*/BCY1 cyr1*Δ/Δ	-	-
PR19	1	*bcy1-E19*/BCY1 cyr1*Δ/Δ	-	-
PR12	2	*Monosomy of ~276 kb of Chr2L cyr1*Δ/Δ	Detected at Chr2: 276,278	ACATCCGTA
PR14	2	*Monosomy of ~276 kb of Chr2L cyr1*Δ/Δ	Detected at Chr2: 276,278	ACATCCGTA
PR18	3	*Monosomy of ~590 kb of Chr2L cyr1*Δ/Δ	Detected at Chr2: 590,175	CATCCG
PR16	3+	*Monosomy of ~557 kb of Chr2L* *Trisomy of ~1342 kb of Chr2 cyr1*Δ/Δ	Detected at Chr2: 1,899,373	GAAG
PR2	3+	*Monosomy of ~557 kb of Chr2L* *Trisomy of ~1239 kb of Chr2 cyr1*Δ/Δ	Detected at Chr2: 1,796,423	CGTACA

† 23-bp telomere repeat sequence, CACCAAGAAGTTAGACATCCGTA

888 **Extended Data Table 2. Potential phosphorylation substrates of Cdc28 and Yck2 during hyphal induction**

Gene	Phosphosite	Description*	Deletion phenotype*
BNI4	S523	Formin; Protein required for wild-type cell wall chitin distribution, morphology, hyphal growth	Hyphal induction: normal
FPK1	T143, S337	Serine/threonine protein kinase	Hyphal induction: normal
ZDS1	S272	Protein with a role in regulating Swe1p-dependent polarized growth	Hyphal induction: normal
INT1	S416, T1214	Bud site selection protein Bud4	Hyphal induction: normal
SOL1	T16	Cell cycle regulator	Hyphal induction: normal
BNI1	S1619	Formin; Role in cytoskeletal organization, cell polarity	Hyphal induction: abnormal
MOB2	S49	Cbk1 kinase activator protein	Hyphal induction: absent
ASK1	S249	Essential subunit of the Dam1 (DASH) complex, which acts in chromosome segregation by coupling kinetochores to spindle microtubules	Inviable

889

890 *Descriptions and deletion phenotypes were obtained from *Candida* Genome Database.

bioRxiv preprint doi: https://doi.org/10.1101/2021.03.08.433668; this version posted March 8, 2021. The copyright holder for this preprint (which was not certified by peer review) is the author/funder, who has granted bioRxiv a license to display the preprint in perpetuity. It is made available under aCC-BY-NC-ND 4.0 International license.

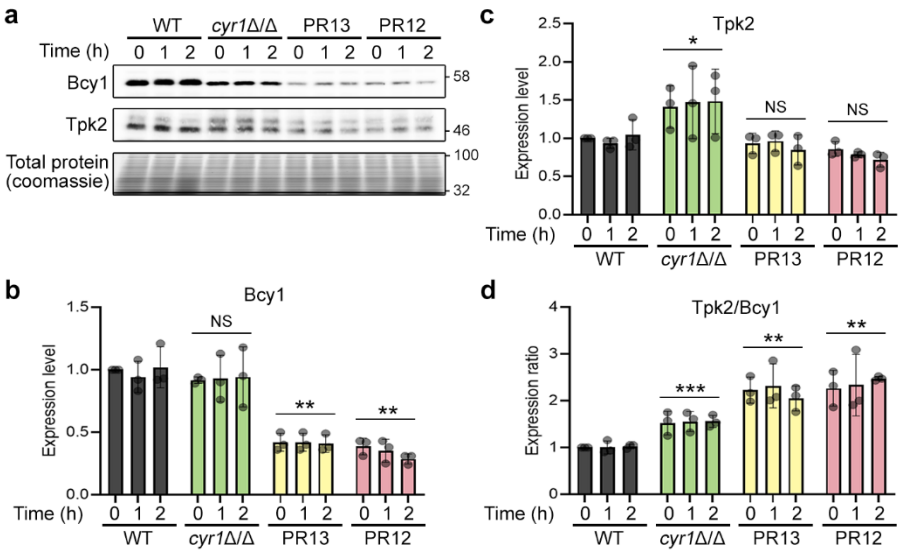

Extended Data Fig. 1. Expression levels of PKA subunits during hyphal induction.

a, Western blot detection of the negative regulatory subunit (Bcy1) and the catalytic subunit (Tpk2) of PKA. Cells were grown at 37°C in liquid galactose medium and then 50 mM GlcNAc was added for 2 h to induce hyphae. The sizes of the protein standards (kDa) are indicated on the right of each blot. Images shown are representative of three independent experiments.

b,c,d, Relative levels of Bcy1 (**b**), Tpk2 (**c**), and TPK2/Bcy1 ratio (**d**) compared to the WT 0-h samples. Shown is the mean ± SD of 3 independent experiments. Expression levels were normalized to total proteins on Coomassie-stained gels. Statistical analysis was performed using one-way ANOVA with Dunnett's multiple comparisons test comparing the strains with the WT; ^{NS} $p > 0.05$, * $p < 0.05$, ** $p < 0.01$, *** $p < 0.001$.

bioRxiv preprint doi: https://doi.org/10.1101/2021.03.08.433668; this version posted March 8, 2021. The copyright holder for this preprint (which was not certified by peer review) is the author/funder, who has granted bioRxiv a license to display the preprint in perpetuity. It is made available under aCC-BY-NC-ND 4.0 International license.

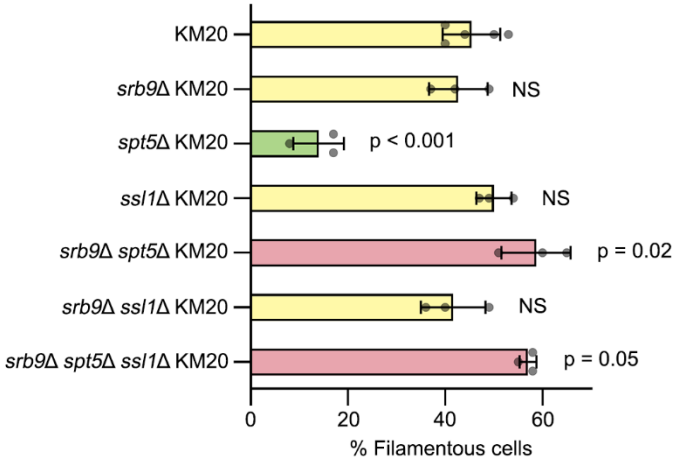

904

905

906 **Extended Data Fig. 2. Gene-mapping analysis of the 10-kb region of chromosome 2 identified a**

907 **role for *SRB9* and *SPT5* in hyphal induction in the PR mutants.**

908 The single, double, and triple heterozygous deletion mutants of *SRB9*, *SPT5*, and *SSL1* were created

909 in KM20 strain background (*Chr2L 90kb→250kbΔ bcy1Δ/BCY1 cyr1Δ/Δ*). The plot shows the percent

910 of filamentous cells in liquid GlcNAc medium at 37°C; green, weak hyphal induction; yellow,

911 intermediate hyphal induction; pink, strong hyphal induction. Statistical analysis was performed using

912 one-way ANOVA with Dunnett's multiple comparisons test comparing the strains with the parental

913 strain; ^{NS} $p > 0.05$.

914

bioRxiv preprint doi: https://doi.org/10.1101/2021.03.08.433668; this version posted March 8, 2021. The copyright holder for this preprint (which was not certified by peer review) is the author/funder, who has granted bioRxiv a license to display the preprint in perpetuity. It is made available under aCC-BY-NC-ND 4.0 International license.

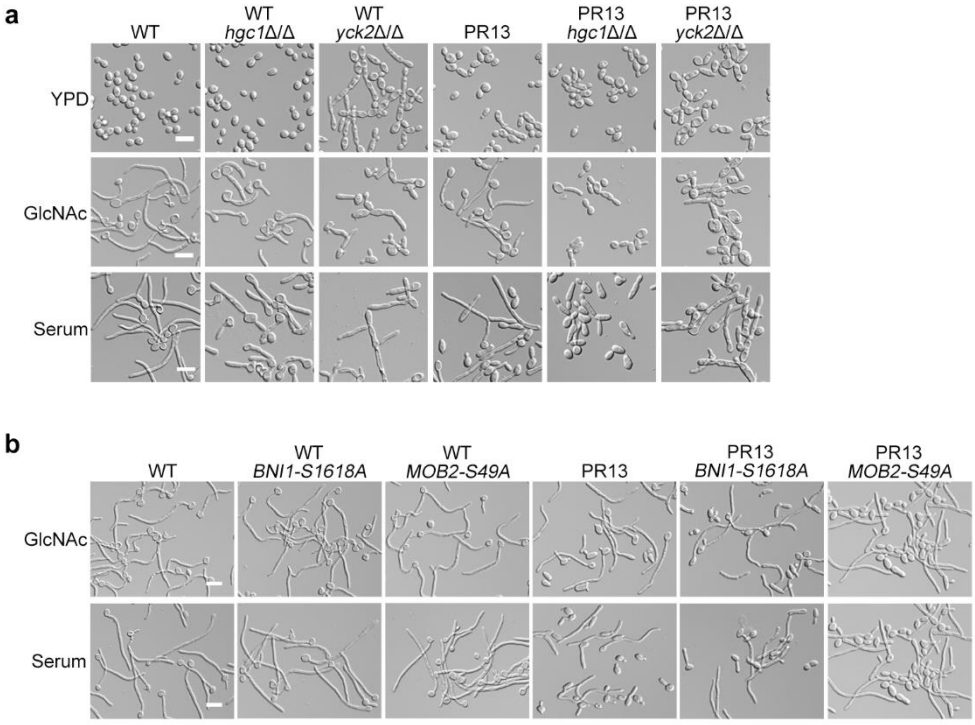

Extended Data Fig. 3. Deletion of Cdc28 cyclin (*HGC1*) and casein kinase 1 (*YCK2*) disrupt normal hyphal growth.

a, Deletion of Cdc28 cyclin (*HGC1*) and casein kinase 1 (*YCK2*) disrupt normal hyphal growth in WT and PR13 backgrounds.

b, Phospho-mutants of Mob2 and Bni1 did not show an obvious defect in hyphal growth.

a,b, The strains indicated at the top were grown in the liquid medium indicated on the left, and then hyphal induction was assessed microscopically. Cells were grown in liquid medium containing 15% serum or 50 mM N-acetylglucosamine (GlcNAc) to induce hyphal growth. Cells were incubated at 37°C for 3 h and then photographed. Scale bar, 10 μm.

bioRxiv preprint doi: https://doi.org/10.1101/2021.03.08.433668; this version posted March 8, 2021. The copyright holder for this preprint (which was not certified by peer review) is the author/funder, who has granted bioRxiv a license to display the preprint in perpetuity. It is made available under aCC-BY-NC-ND 4.0 International license.

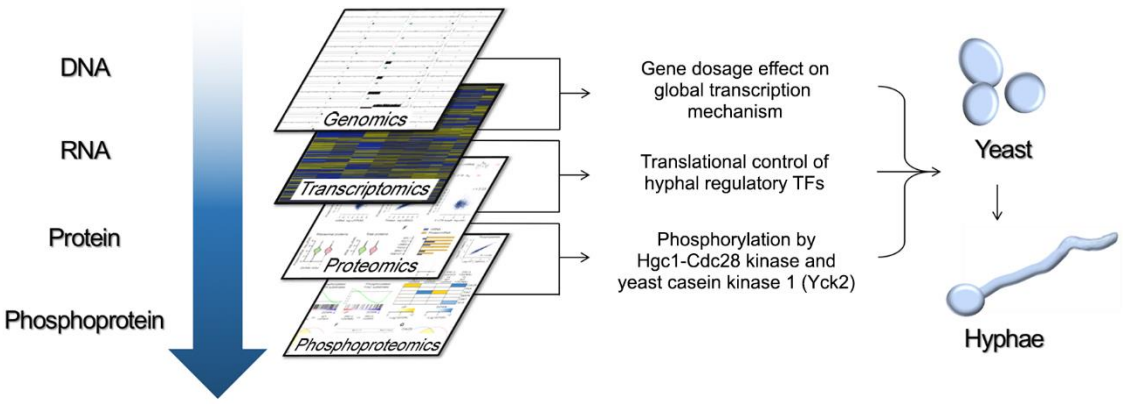

927

928

929 **Extended Data Fig. 4. Integrative multi-omics profiling revealed new pathways that induce *C.***

930 ***albicans* hyphal formation in a cAMP-independent manner.**

931 We gained mechanistic insights into hyphal morphogenesis, by performing integrative multi-omics

932 profiling in *C. albicans*. Genetic changes in PR mutants were identified by performing genome

933 analysis, gene-mapping by CRISPR-Cas9, and transcriptome analysis. These studies showed that

934 gene dosage effects on *BCY1* (negative regulator of PKA) and global transcription mechanisms

935 promoted hyphal growth in the absence of cAMP. Integrating transcriptomic and proteomic data

936 revealed that translation rate of some hyphal regulatory TFs increased dramatically during hyphal

937 induction while their mRNA levels did not, suggesting a novel mechanism of translational regulation

938 promotes hyphal growth. We revealed that phosphorylation by Hgc1-Cdc28 kinase and yeast casein

939 kinase 1 (Yck2) plays a crucial role in hyphal induction by performing parallel comparisons of protein

940 expression and phosphorylation. In conclusion, hyphal morphogenesis is regulated by multiple

941 processes in a cAMP-independent manner.

942